Available online at www.sciencedirect.com
SCIENCE DIRECT®
Journal of Nuclear Materials 349 (2006) 195–233
journal of nuclear materials
www.elsevier.com/locate/jnucmat

Review

A literature review of reactions and kinetics of lithium hydride hydrolysis

C. Haertling *, R.J. Hanrahan Jr., R. Smith

Material Science and Technology Division, Los Alamos National Laboratory, P.O. Box 1663, Los Alamos, NM 87545, USA

Received 8 February 2005; accepted 4 October 2005

Abstract

Studies of lithium hydride (LiH) reactions with H_2O are reviewed in this paper. We discuss reaction products that are formed and the reaction kinetics involved. For discussion purposes, the studies are roughly categorized as reactions between LiH and H_2O in low and higher concentration regimes, as well as reactions between LiH hydrolysis products. Both LiH and H_2O can exist in many structural or phase variations and can contain various impurities, all of which may affect products and kinetics.
Published by Elsevier B.V.

PACS: 82.20

Contents

* Corresponding author.
E-mail address: chaert@lanl.gov (C. Haertling).

0022-3115/$ - see front matter Published by Elsevier B.V.
doi:10.1016/j.jnucmat.2005.10.005

1. Introduction

Lithium hydride (LiH) is a compound that has spawned a great deal of research. The first reasonably stoichiometric material was prepared in 1896 by Guntz [1]. Hydrolysis studies of the material followed shortly; indeed, papers in this review are drawn from a century of studies and from many different countries. The long term interest in LiH stems from its unique applications, including use as a neutron shield or moderator, as a fusion reactor fuel, as a hydrogen gas source, and as a heat storage material. Furthermore, LiH has some distinctive qualities that make it an interesting compound for study: it has an extremely simple electronic structure, it is a strong reducing agent, and it is a target for producing tritium.

Lithium hydride is highly reactive with water, which can cause difficulties in handling and use. However, the hydrolysis reaction has also sparked interest as a method of hydrogen production. Reactions can potentially continue for years at ambient or room temperature (RT) conditions as initial reaction products continue to react amongst themselves.

Lithium hydride hydrolysis reaction studies often involve isotopic variations of the elements in the LiH or H_2O reactants. For example, Li may be in the form of Li^6 or Li^7. The natural isotopic amounts for Li are 7.5 at.% Li^6 with the balance as Li^7. Lithium hydride containing Li^6 is used in several studies reviewed here, as this isotope is more readily available to some researchers. However, Li isotopes will not be identified in this paper, as the specification here is not greatly important, and because Li isotopes are usually not named in reviewed papers. H may be in the form of H^1, H^2, or H^3 and will be specified here. H^1, or protium, is designated H; H^2, or deuterium, is designated D; and H^3, or tritium, is designated T. General discussion of lithium hydride that could include various hydrogen isotopes (apparent from the context), will use the term LiH. Hydrogen isotopes have been used to trace the origin of reaction products in hydrolysis reactions. Oxygen isotopes could also be used to track reactions, but this method has not been found in the LiH hydrolysis literature.

This paper reviews the literature on LiH hydrolysis reaction products and kinetics; our intent is to clarify what work has been done and how these studies are related. Although a number of studies encompassing LiH hydrolysis studies have been completed, the multitude of material types, H_2O forms and isotopics, sample environments, and experimental techniques, as well as the variety of units used to report the findings, can be daunting. We have attempted to be inclusive in this review. However, studies in which products or kinetics were not analyzed, e.g., studies to determine heats of reaction or solubility limits, are mentioned only when pertinent to the discussion and are not specifically detailed. A series of studies on LiH hydrolysis were completed by Oates [53], Segal [54], and Mather [55] in the United Kingdom, but were unavailable to the authors of the present work and were therefore not reviewed. There are studies of Li metal in which LiH is formed, as well as other hydrolysis products. Discussion of these studies is not included in this paper, but should be reviewed by the interested reader since the results could be relevant to LiH corrosion.

2. Hydrolysis reaction products

Solid compounds that have been experimentally identified as direct or indirect products of reactions between LiH and H_2O are Li_2O, LiOH, $LiOH \cdot H_2O$, and Li_3O_2. Table 1 lists the structural characteristics of these products. LiOH (and its monohydrate, $LiOH \cdot H_2O$) are the most prevalent products (i.e. products most frequently identified in studies as well as identified as equilibrium products in phase diagrams) from RT and pressure reactions of LiH with ambient concentrations of H_2O. Further Li compounds have been calculated to exist in the Li–O–H phase diagram, but have not been observed experimentally from a LiH hydrolysis route.

Impurities, either within the LiH starting material, H_2O, or the gaseous environment surrounding

Table 1
LiH hydrolysis products and structural information [2–4]

Compound	Lattice	Space group	Lattice parameters						Molar volume, cm^3/mol	Density[a] (g/cm^3)
			a, nm	*b*, nm	*c*, nm	α, deg	β, deg	γ, deg		
$Li^{nat.\ ab.}H$	Cubic	*Fm-3m* (225)	40.511	40.511	40.511	90	90	90	10.26	0.77
Li^7H	Cubic	*Fm-3m* (225)	40.484	40.484	40.484	90	90	90	10.26	0.77
Li^6H	Cubic	*Fm-3m* (225)	40.843	40.843	40.843	90	90	90	10.26	0.68
Li^7D	Cubic	*Fm-3m* (225)	40.695	40.695	40.695	90	90	90	10.26	0.87
Li^6D	Cubic	*Fm-3m* (225)	40.704	40.704	40.704	90	90	90	10.26	0.78
Li^7T	Cubic	*Fm-3m* (225)	40.636	40.636	40.636	90	90	90	10.26	0.97
Li^6T	Cubic	*Fm-3m* (225)	40.642	40.642	40.642	90	90	90	10.26	0.88
LiOH	Tetragonal	*P4/nmm* (129)	35.49	35.49	43.34	90	90	90	16.52	1.45
Li_2O	Cubic	*Fm-3m* (225)	46.19	46.19	46.19	90	90	90	7.422	2.01
$LiH \cdot H_2O$	Monoclinic	*C2/m* (12)	76.4	84.4	32.4	90	110.9	90	27.79	1.51
Li_3O_2	Orthorhombic	n/a	108.4	128.4	103.6	90	90	90	n/a	n/a

nat. ab. = natural abundance of Li isotopes, which is 92.5 at.% Li^7 and 7.5 at.% Li^6; all values for this compound are calculated.
n/a = not available.
[a] Calculated theoretical density.

the reactants, are often present during hydrolysis. Therefore, hydrolysis reactions may include reactions with impurity species. Some of these species could affect the products formed or the reaction rate. Table 2 lists the gases that are typically present in air. When H_2O is exposed to air, these impurities are dissolved in the H_2O. Table 2 also lists the solubilities of air gases dissolved in H_2O at RT. Note that solubility of CO_2 in H_2O is greater than that of other gases by an order of magnitude. LiH can react with CO_2, as well as several of the other gases such as O_2 and N_2 [6,7].

2.1. Reactions between LiH and H_2O

The principal product of LiH hydrolysis at RT and ambient pressure is LiOH. Li_2O has also been experimentally observed as a layer between the LiOH and bulk LiH (or LiD) [8–11], and has been inferred or suggested to be present by several other researchers [12–14]. The generalized hydrolysis layer structure can be designated by $LiOH/Li_2O/LiH$ (bulk). Many reports do not mention Li_2O; however, it is thought to form a very thin layer (~100 Å) at RT and would be difficult to detect [14]. Because many studies were not concerned with identifying the reaction product, but with determining reaction kinetics or some other property, the identity of reaction products was often presumed rather than experimentally identified. Fig. 1 shows a schematic of a commonly observed product layer structure for RT and pressure LiH hydrolysis reactions.

Table 2
Air composition along with gas solubilities in H_2O at 25 °C and 101.3 kPa [5]

Gas	Content (vol.%)	Solubility in H_2O (mole fraction)
N_2	78.084	1.274×10^{-5}
O_2	20.948	2.501×10^{-5}
Ar	0.934	2.748×10^{-5}
CO_2	0.0314	7.070×10^{-4}
Ne	0.00182	8.395×10^{-6}
He	0.000524	7.044×10^{-6}
CH_4	0.000200	2.806×10^{-5}
Kr	0.000114	5.041×10^{-5}
H_2	0.0000500	1.455×10^{-5}
Xe	0.0000087	9.051×10^{-5}

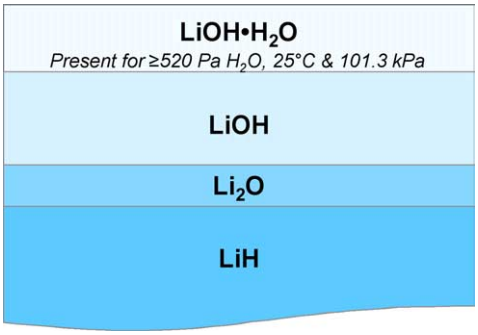

Fig. 1. Schematic of LiH hydrolysis product layers that has been observed and proposed for LiH hydrolysis reactions at room temperature (RT) and pressure (101.3 kPa) and with typical quantities of H_2O in air [8,9,12,14]. The product layers might react amongst themselves over long periods of time (years).

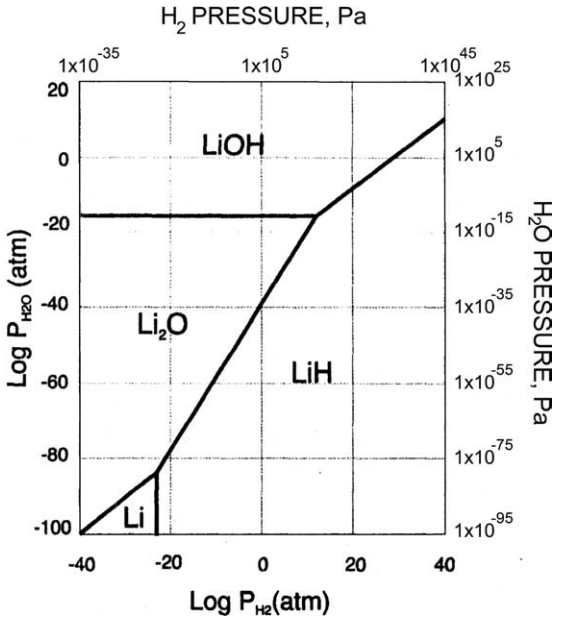

Fig. 2. H_2O and H_2 pressure phase diagram of Li–O–H phases at RT. Ambient partial pressure of H_2 at 25 °C is 5.1×10^{-4} Pa or log (pressure H_2) = −3.3 Pa [14].

An Li–O–H phase diagram at varying H_2O and H_2 partial pressures at RT is shown in Fig. 2 [14]. The diagram shows that Li_2O is the thermodynamically stable oxygen containing phase at H_2 partial pressures greater than ambient ($\sim 1 \times 10^{15}$ Pa) to well below ambient (ambient $H_2 = 5.1 \times 10^{-4}$ Pa), and at very low H_2O partial pressures ($\leqslant 1 \times 10^{-13}$ Pa). At higher H_2O pressures, LiOH is thermodynamically stable. For LiOH to be adjacent to LiH, however, an intervening layer is required in which H_2O activities are graduated. The Li_2O layer serves this purpose, leading to the layer structure described in Fig. 1. Similar phase diagrams have been determined by other researchers [15,16]. Unfortunately, the published diagrams do not contain units, however, the relative positions of phases are the essentially the same. The phase diagram by Broughton shows the largest range of H_2 and H_2O pressures and includes Li_2O_2 and LiO_3 phases at very low H_2 pressures and high H_2O pressures. Trace quantities of $Li_2(OH)_2$ and $Li_3(OH)_3$ have also been reported as products of reaction between Li_2O and ~13 Pa of H_2O at temperatures of ~830–1130 °C [17].

Although the existence of an Li_2O layer between LiH and LiOH is not strongly disputed, confusion exists regarding the order in which reactions take place to form this layer. For example, hydrolysis could occur as follows (analogous reactions could also occur for LiD or D_2O):

Hydroxide first

$$LiH_{(s)} + H_2O_{(g)} \rightarrow LiOH_{(s)} + H_{2(g)}$$
$$\Delta H_{25\,^\circ C} = -147\ \text{kJ} \quad [18] \qquad \text{(R1)}$$
$$LiOH_{(s)} + LiH_{(s)} \rightarrow Li_2O_{(s)} + H_{2(g)}$$
(at LiH/LiOH interface)
$$\Delta H_{25\,^\circ C} = -22.9\ \text{kJ} \quad [6] \qquad \text{(R2)}$$

or by the following set of reactions:

Oxide first

$$2LiH_{(s)} + H_2O_{(g)} \rightarrow Li_2O_{(s)} + 2H_{2(g)}$$
$$\Delta H_{25\,^\circ C} = -339\ \text{kJ} \quad [12] \qquad \text{(R3)}$$
$$Li_2O_{(s)} + H_2O_{(g)} \rightarrow 2LiOH_{(s)} \text{ (at surface)}$$
$$\Delta H_{25\,^\circ C} = -124\ \text{kJ} \quad [12] \qquad \text{(R4)}$$

Note: The heats of reaction ($\Delta H_{25\,^\circ C}$) for the above and all subsequent reactions were calculated from heat of formation values at ambient pressure in the JANAF Thermochemical Tables, 1971 [19], and other chemistry resources.

In the reaction sets above, the second reactions consume the products of the first reactions, but do not necessarily react completely. For example, in the oxide first case, Li_2O is thought to form LiOH, but some Li_2O would remain, to form a layer between the LiH and LiOH as discussed previously. In the hydroxide first case, LiOH and H_2O are thought to form Li_2O at the LiOH/LiH interface. At RT, the reactions to form Li_2O from LiOH are so slow that, in practice, the LiOH is the end product [20]. Elevated temperatures increase the rate of the reaction [6,21]. The stability of LiOH has been a subject of several studies, which will be discussed later. In both the hydroxide first and oxide first cases, the solid products are Li_2O and LiOH, while the gas products are H_2. There is little in terms of products to distinguish between the cases (unless isotopic tracing is used). Determining which product forms first is therefore difficult, but has in fact been addressed [12,13].

While the order of product formation is not easily distinguished, the reactions have significantly different heats of reaction. The heat of reaction for the oxide first forming reaction, Rn. (reaction) (R3), is much more negative than the heat of reaction for the hydroxide first forming reaction, Rn. R1, (−339 kJ for the former and −147 kJ for the latter); hence the 'oxide first' reaction is thermodynamically favored.

The use of hydrogen isotopes in hydrolysis studies can lead to some determinations of reaction mechanisms. The hydroxide first and oxide first reaction sets are shown with LiD and H_2O used as reactants in the first case and LiH and D_2O used in the second case.

Using LiD and H_2O:

Hydroxide first

$$LiD + H_2O \rightarrow LiOH + HD(\text{or } LiOD + H_2) \quad (R5)$$

$$LiOH + LiD \rightarrow Li_2O + HD(\text{or } Li_2O + D_2) \quad (R6)$$

Oxide first

$$2LiD + H_2O \rightarrow Li_2O + H_2 + D_2 \ (\text{or } 2HD) \quad (R7)$$

$$Li_2O + H_2O \rightarrow 2LiOH \quad (R8)$$

Using LiH and D_2O:

Hydroxide first

$$LiH + D_2O \rightarrow LiOD + HD \ (\text{or } LiOH + D_2) \quad (R9)$$

$$LiOD + LiH \rightarrow Li_2O + HD \ (\text{or } Li_2O + H_2) \quad (R10)$$

Oxide first

$$2LiH + D_2O \rightarrow Li_2O + H_2 + D_2 \ (\text{or } 2HD) \quad (R11)$$

$$Li_2O + D_2O \rightarrow 2LiOD \quad (R12)$$

In the oxide first scenarios, only LiOH can result from the reaction of LiD and H_2O, and only LiOD can result from the reaction of LiH and D_2O. However, either hydroxide product could potentially result from the hydroxide first reaction set. Therefore, if LiOH resulted from the reaction of LiH and D_2O, or if LiOD resulted from the reaction of LiD and H_2O, the oxide first reaction mechanism would be excluded.

Tetenbaum et al. [22] and Norman and Hightower [23] showed that at elevated temperatures (~300–1000 °C), LiOH and Li_2O are mutually soluble up to a limit. Fig. 3 is a plot of solubility for these compounds in each other as a function of temperature and H_2O pressures. LiOH solubility in Li_2O increases with increasing H_2O partial pressure and temperature. Visual extrapolation of the data indicates that the solubility is minimal at very low H_2O levels near RT and ambient pressure. Krikorian expanded upon this data set and developed a phase diagram for LiOH and Li_2O at temperatures ranging from ~200 to 1700 °C [24]. The phase diagram is shown in Fig. 4. Myers advocated the concept that the Li_2O is present in the form of a layer, rather than mixed in with the LiOH [11]. He based this view on studies at elevated temperatures that

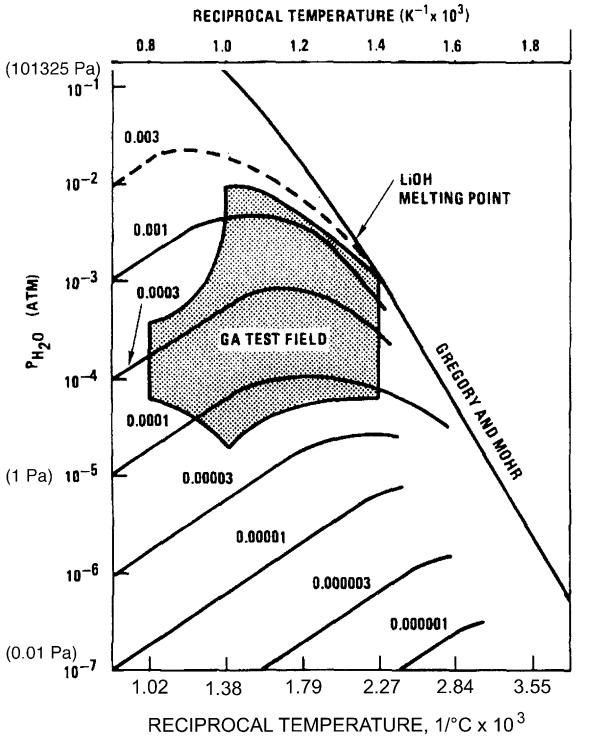

Fig. 3. Solubility of LiOH in Li_2O at various temperatures and H_2O vapor pressures. The numbers adjacent to the curves are LiOH concentrations in Li_2O. The shaded area is the range used in experiments by Norman and Hightower [23]. SI units were added by the present authors.

showed Li_2O and LiOH layers [10,11], as well as an argument that the large crystallographic volume differences between the two compounds made a mixture unlikely.

The equilibrium partial pressure of H_2O over Li_2O–LiOH at elevated temperatures that was measured or calculated by several researchers was compiled by Terai et al. [25], and is shown in Fig. 5. The figure shows the H_2O concentrations at which reactions between LiOH, Li_2O and H_2O should occur for elevated temperatures (~300–1150 °C). Below the curves in the figure (low H_2O concentration and high temperature regimes), H_2O and Li_2O are present; above the curves (in high H_2O concentration and low temperature regimes), the materials react to form LiOH by the reaction $Li_2O + H_2O \rightarrow 2LiOH$.

Above H_2O pressures of 523 Pa at 25 °C and environmental pressures of 101.3 kPa (16.4% relative humidity at RT and ambient pressure), the monohydrate, $LiOH \cdot H_2O$, forms when LiH

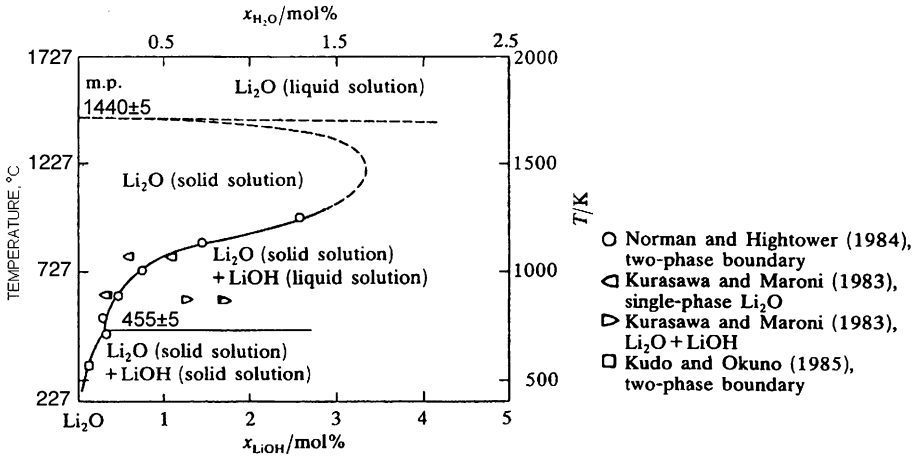

Fig. 4. Phase diagram of the Li_2O–LiOH system in the Li_2O rich region [24]. Celsius units were added by the present authors.

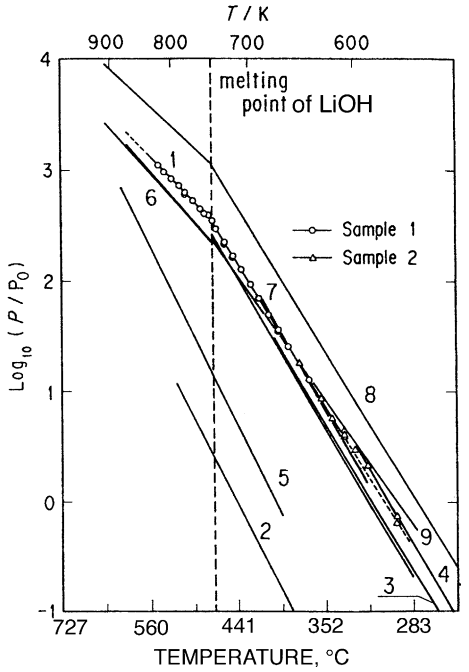

Fig. 5. Equilibrium partial pressures of H_2O over Li_2O–LiOH mixtures; 1 = Terai, 1989, 2 = Ditmars et al., 1953, 3 = Gregory et al., 1955, 4 = Berkowitz et al., 1960, 5 = Yoshida et al., 1982, 6 = Tetenbaum et al., 1984, 7 = Takeshita et al., year, 8 = calculated from JANAF Thermochemical Tables, 1991, 9 = Munakata et al., 1989 [25]. Below the curves, Li_2O and H_2O are present; above the curves, LiOH is present. The present authors added Celsius units.

hydrolyzes [26]. It is useful to keep these conditions in mind while reviewing LiH hydrolysis literature. Lithium hydroxide monohydrate could form by either of the following suggested reactions:

$$LiH_{(s)} + 2H_2O_{(g)} \rightarrow LiOH \cdot H_2O_{(s)} + H_{2(g)}$$
$$\Delta H_{25\,^\circ C} = -215\ \text{kJ} \quad [15] \qquad \text{(R13)}$$

or

$$LiOH_{(s)} + H_2O_{(g)} \rightarrow LiOH \cdot H_2O_{(s)}$$
$$\Delta H_{25\,^\circ C} = -68.8\ \text{kJ} \quad [27] \qquad \text{(R14)}$$

Experimental work to date points to the second reaction taking place, in which LiOH is formed as an intermediary product from LiH hydrolysis and is then consumed as a reactant. Dinh et al. [27] used temperature programmed desorption (TPD) (a technique in which materials are heated and the evolved gases analyzed by mass spectrometry), to show that both LiOH and $LiOH \cdot H_2O$ films were present as products from hydrolysis. The simultaneous presence of both phases was also shown by Smyrl et al. [7] and Powell et al. [28]. Balooch et al. [16], furthermore, showed that the $LiOH \cdot H_2O$ layer forms on the surface of the LiOH layer. In a layer structure of hydrolysis products, the LiOH layer should serve as a layer of graduated H_2O activity between the lower activity of an Li_2O phase and the greater H_2O activity of an $LiOH \cdot H_2O$ phase, as is consistent with Fig. 1. While experimental observations support Rn. (R14), the phase diagram by Broughton [15] indicates that LiH may potentially form directly from LiH at 25 °C with very high H_2 and H_2O pressures.

Some researchers have studied LiH hydrolysis with very high H_2O concentrations, where the final products are ions in aqueous solutions. At very high H_2O to LiH ratios (e.g. solid LiH submerged in H_2O), the following reaction set occurs:

$$LiH_{(s)} + H_2O_{(l)} \rightarrow LiOH_{(aq)} + H_{2(g)} \quad [29] \qquad (R15)$$

$$LiOH_{(aq)} + H_2O_{(g)} \rightarrow Li^+_{(aq)} + OH^-_{(aq)} \quad [29] \qquad (R16)$$

The aqueous solubility limit of LiOH is 12.8 g/L (9.6 $LiOH/H_2O$ molar ratio) at 20 °C [30], and thus, H_2O added to LiOH at a molar ratio of <9.6 will produce Li^+ and OH^-. From this information, the aqueous solubility limit of LiH at 20 °C may be calculated as 6.40 g/L; a LiH/H_2O molar ratio of <4.8 will produce Li^+ and OH^-.

2.2. Reactions between LiH hydrolysis products

The desire to understand long-term, slow equilibration hydrolysis reactions has resulted in several studies on LiOH. LiOH either reacts with LiH, or decomposes, to form Li_2O by the following:

$$LiOH_{(s)} + LiH_{(s)} \rightarrow Li_2O_{(s)} + H_{2(g)}$$
$$\Delta H_{25\,^\circ C} = -22.9\ \text{kJ} \quad [2] \qquad (R17)$$

$$2LiOH_{(s)} \rightarrow Li_2O_{(s)} + H_2O_{(g)}$$
$$\Delta H_{25\,^\circ C} = 124\ \text{kJ} \quad [21] \qquad (R18)$$

The formation of Li_2O has typically been studied at elevated temperatures; however, Li_2O should form even at RT [6,31].

Stecura [3] showed that trilithium dioxide, Li_3O_2, forms from LiOH at elevated temperatures (up to 730 °C) and lowered pressures ($\sim 2 \times 10^{-3}$ Pa). This compound is formed by decomposition as follows:

$$6LiOH_{(s)} \rightarrow 2Li_3O_{2(s)} + 2H_2O_{(g)} + H_{2(g)} \quad [3] \qquad (R19)$$

Further reactions between LiOH and other LiH hydrolysis products have been mentioned in the literature, specifically:

$$LiOH_{(s)} + H_{2(g)} \rightarrow LiH_{(s)} + H_2O_{(g)}$$
$$\Delta H_{25\,^\circ C} = 147\ \text{kJ} \quad [32] \qquad (R20)$$

and

$$LiOH \cdot H_2O_{(g)} + LiH_{(s)} \rightarrow 2LiOH_{(s)} + H_{2(g)}$$
$$\Delta H_{25\,^\circ C} = -77.7\ \text{kJ} \quad [33] \qquad (R21)$$

Rn. (R20) is the reverse reaction of Rn. (R1) (and has a positive heat of reaction value at RT). Shpil'rain stated that the latter reaction, Rn. (R21), had been studied as a source of H_2 fuel for rockets. The products of these reactions could, of course, react to form further reaction products.

The reaction between the hydrolysis product Li_2O and another product, H_2, has been studied for the potential application of using Li_2O as a breeder blanket material for fusion reactors (produces T by the reaction $Li^6 + n \rightarrow He + T$). The reactions are the reverse of reactions given above for the formation of Li_2O.

$$Li_2O_{(s)} + 2H_{2(g)} \rightarrow 2LiH_{(s)} + H_2O_{(g)}$$
$$\Delta H_{25\,^\circ C} = 170\ \text{kJ} \quad [32] \qquad (R22)$$

$$Li_2O_{(s)} + H_{2(g)} \rightarrow LiOH_{(s)} + LiH_{(s)}$$
$$\Delta H_{25\,^\circ C} = 22.9\ \text{kJ} \quad [34] \qquad (R23)$$

Studies of these reactions typically used temperatures $\geqslant$400 °C and focused on a particular application; therefore, parameters for the experiments (e.g. H_2 concentrations) were optimized for the application and are not necessarily realistic for studying reactions that might occur between hydrolysis products. Nevertheless, some studies of these reactions are included here to demonstrate potential reactions amongst LiH hydrolysis products.

3. Studies of LiH hydrolysis reaction products

We have grouped the following studies of LiH hydrolysis by the types of reaction products produced at different experimental conditions. The first groups are 'low-H_2O concentration' and 'high-H_2O concentration' regimes. At RT and ambient pressures, the low H_2O concentration regime reflects a H_2O concentration range in which the prevalent hydrolysis product is Li_2O, while in the high regime, LiOH and $LiOH \cdot H_2O$ are the prevalent hydrolysis products. These experiments are summarized in Table 3. A final group is 'LiH reaction products' that includes studies on reactions amongst hydrolysis reaction products. These experiments are summarized in Table 4. The distinctions between groups are not always clear and may overlap in some cases. It should be noted that study of an unoxidized LiH surface is difficult at best, due to the extremely strong reactivity of LiH with H_2O, and therefore essentially all studies of LiH include an oxidized surface (with the possible exception of LiH crystal cleaved in ultrahigh vacuum just prior to study).

In viewing figures taken from the references, the reader should be aware that a variety of notations were used. Specifically, different authors have reported H_2O concentrations in different units. We have attempted to convert all H_2O concentrations to the same unit for comparisons; we present H_2O concentrations in pressure units, as that is the most

Table 3
Summary of experiments for reactions between LiH and H_2O

exp. #, step #	SAMPLE MATERIAL	SAMPLE FORM	EXPOSURE ENVIRONMENT	H_2O PURITY	H_2O CONTENT (Pa)	EXPOSURE PROCESS	EXPOSURE TIME	EXPOSURE TEMPERATURE	ANALYSIS TECHNIQUES	PRODUCTS IDENTIFIED	KINETIC EXPRESSIONS
* = converted from relative humidity value using HCON software from General Eastern Instruments. The following values were used: 25°C (ambient) or applicable temperature value, 101.3 kPa (ambient) or applicable pressure value, and 29 g/mole (air) or applicable molecular weight value; ° = converted from ppm value in literature with no mention of unit, ppmv is assumed; n/m = not mentioned in the literature, RT = room temp.											
–A note on H_2O content units: Different authors have reported H_2O contents in different units. We have attempted to convert all H_2O contents to the same unit for comparisons. The reviewers would prefer units of mole, however literature authors have frequently reported H_2O contents in pressure units without providing additional information for conversions to moles. Therefore, we present H_2O contents in pressure units as that is the most accessible unit for comparison.											
Balooch, Dinh, Calef; 2002											
exp. 1	LiD	single crystal	vacuum	n/m	$1.3x10^{-5}$	single dose	~4 min	RT-~230°C, LiH heated	MMBMS, AES	LiOH (no experimental identification shown)	
exp. 2	LiD	single crystal	N_2, pressure n/m	n/m	2338* assuming H_2O temp @ 20°C	continuous	n/m	~20-175°C, method n/m	gravimetry	none	$7.6x10^{15}$ uptake of O atoms/second
exp. 3	LiD	single crystal	air, ambient pressure	H_2O from air	1584*	continuous	≤1400 min	n/m, assume RT	AFM	LiOH, LiOH•H_2O (identified from hardness data)	0.363 nm/min for LiOH•H_2O, 21.8 nm/min for LiOH
exp. 4	LiD	single crystal	air, ambient pressure	H_2O from air	1584*	continuous	≤1400 min	RT	SEM	none	Initial rise, then linear behavior for ~μms thickness; ~20 μm in 1375 min
Beutler, Brauer, Junger; 1936											
exp. 1	LiH	polyxtal powder	vacuum	D_2O	n/m, liquid	n/m	n/m	n/m, assume RT	UV absorption	D_2, H_2, HD	
Broughton; 2001											
exp. 1	LiH	polyxtal powder	Ar @ glovebox pressure	n/m	550*	flowing @ 500 mL/min	10000 min	20-25°C	gravimetry	none	Initial rise, then linear behavior; ~0.5 mg/min
exp. 2	LiH	polyxtal powder	Ar @ glovebox pressure	n/m	1900*	flowing @ 500 mL/min	~7000 min	20-25°C	gravimetry	none	Initial rise, then linear behavior; 1.2 mg/min
exp. 3	LiH	polyxtal pellet	Ar @ glovebox pressure	n/m	630*	flowing @ 1000 mL/min	~1200 min	37-41°C, gas heated	gravimetry	none	$R=-0.8560t^2+1.338t-0.7325t+0.2002$
exp. 4	LiH	polyxtal pellet	Ar @ glovebox pressure	n/m	1500*	flowing @ 1000 mL/min	~1200 min	37-41°C, gas heated	gravimetry	none	$R=-0.6810t^2+1.159t-0.6825t+0.2093$
exp. 5	LiH	polyxtal pellet	Ar @ glovebox pressure	n/m	2600*	flowing @ 1000 mL/min	~1200 min	37-41°C, gas heated	gravimetry	none	$R=-0.5947t^2+0.9395t-0.5448t+0.2059$
exp. 6	LiH	polyxtal pellet	Ar @ glovebox pressure	n/m	1300*	flowing @ 1000 mL/min	~7200 min	33°C, gas heated	gravimetry	none	$L=-0.0002t+0.0034$
exp. 7	LiH	polyxtal pellet	Ar @ glovebox pressure	n/m	930*	flowing @ 1000 mL/min	~7200 min	39°C, gas heated	gravimetry	none	$L=-0.0002t+0.0034$
exp. 8	LiH	polyxtal pellet	Ar @ glovebox pressure	n/m	1300*	flowing @ 1000 mL/min	~7200 min	57°C, gas heated	gravimetry	none	$L=-0.0002t+0.0034$
exp. 9	LiH	fine polyxtal powder	Ar @ glovebox pressure	n/m	1300*	flowing @ 1000 mL/min	~7200 min	33°C, gas heated	gravimetry	none	
exp. 10	LiH	coarse polyxtal powder	Ar @ glovebox pressure	n/m	1300*	flowing @ 1000 mL/min	~7200 min	33°C, gas heated	gravimetry	none	
exp. 12	LiH	fine powder polyxtal pellet	Ar @ glovebox pressure	n/m	1300*	flowing @ 1000 mL/min	~7200 min	33°C, gas heated	gravimetry	none	
exp. 13	LiH	fine powder polyxtal pellet	Ar @ glovebox pressure	n/m	950*	flowing @ 1000 mL/min	~7200 min	39°C, gas heated	gravimetry	none	
exp. 14	LiH	fine powder polyxtal pellet	Ar @ glovebox pressure	n/m	950*	flowing @ 1000 mL/min	~7200 min	39°C, gas heated	gravimetry	none	
exp. 15	LiH	fine powder polyxtal pellet	Ar @ glovebox pressure	n/m	950*	flowing @ 1000 mL/min	~7200 min	39°C, gas heated	gravimetry	none	
Buchanan, Bowen; 1960											
exp. 1, st. 1	LiH	as received polyxtal powder	–	–	–	–	–	–	IR	LiOH, LiOH•H_2O	
st. 2			vacuum	–	–	continuous	15 min	300°C	IR	LiOH, less LiOH•H_2O	
st. 3		n/m	–	H_2O, from air	2852 Pa*	continuous	n/m	n/m, assume RT	IR	LiOH, more LiOH•H_2O	
Cecala, Shaw, Leckey; 2001											
exp. 1	LiH, 5 g	polyxtal pellet	n/m, assume air	n/m	4.5 L, liquid	intimate mixing		25-95°C, solution temp measured	solution conductivity, visual for gas bubbling	Li^+, OH^-, H_2 presumed	$k = Ae^{\frac{-E}{RT}}$
Cristy; 1987											
exp. 1	LiH	single crystal	vacuum	D_2O	347	single dose	300 sec	n/m, assume RT	SIMS	LiOD/Li_2O/LiH (bulk)	

R = weight gain rate (% mass increase/day)
t = time (hours)

L = reciprocal of LiH loss (1/mmol of LiH)
t = time (hours)

k = rate constant = 1.53×10^{-3} to 3.05×10^{-3} cm/s
A = preexponential factor = 1.72×10^{-4} cm/s
E = activation energy = –6.7 kJ/mol
R = gas constant, kJ/mol·K
T = temperature, K

exp. #, step #	SAMPLE MATERIAL	SAMPLE FORM	EXPOSURE ENVIRONMENT	H_2O PURITY	H_2O CONTENT (Pa)	EXPOSURE PROCESS	EXPOSURE TIME	EXPOSURE TEMPERATURE	ANALYSIS TECHNIQUES	PRODUCTS IDENTIFIED	KINETIC EXPRESSIONS
DeVries; 1968											
exp. 1	LiH, 0.10-0.34 g	n/m, assume polyxtal powder	n/m	n/m	5 ml liquid	intimate mixing	n/m	21°C	pressure change		
exp. 2	LiH, 1 g	n/m, assume polyxtal powder	n/m	n/m	25 ml liquid	intimate mixing	n/m	21°C	pressure change	H_2 presumed	
exp. 3	LiH, 6 g	coarse polyxtal powder	n/m	"fresh" water	750 ml liquid	intimate mixing	6 min	21°C	pressure change	H_2 presumed	90% H_2 generated in 1 min
exp. 4	LiH, 15 g	coarse polyxtal powder	n/m	"fresh" water	750 ml liquid	intimate mixing	6 min	21°C	pressure change	H_2 presumed	77% H_2 generated in 1 min
exp. 5	LiH, 30 g	coarse polyxtal powder	n/m	"fresh" water	750 ml liquid	intimate mixing	6 min	21°C	pressure change	H_2 presumed	80% H_2 generated in 1 min
exp. 6	LiH, 30 g	coarse polyxtal powder	n/m	"fresh" water	500 ml liquid	intimate mixing	6 min	21°C	pressure change	H_2 presumed	69% H_2 generated in 1 min
exp. 7	LiH, 15 g	fine polyxtal powder	n/m	"fresh" water	750 ml liquid	intimate mixing	6 min	21°C	pressure change	H_2 presumed	104% H_2 generated in 1 min
exp. 8	LiH, 15 g	fine polyxtal powder	N_2 pressurized to 47.9 kPa	seawater	750 ml liquid	intimate mixing	6 min	21°C	pressure change	H_2 presumed	120% H_2 generated in 1 min
exp. 9	LiH, 15 g	fine polyxtal powder	N_2 pressurized to 47.9 kPa	seawater + 7.5 g motor oil	750 ml liquid	intimate mixing	6 min	21°C	pressure change	H_2 presumed	57% g H_2 generated in 1 min
exp. 10	LiH, 7.5 g	fine polyxtal powder	n/m	seawater + 3.7 g motor oil	750 ml liquid	intimate mixing	6 min	21°C	pressure change	H_2 presumed	70% H_2 generated in 1 min
exp. 11	LiH, 7.5 g	fine polyxtal powder	n/m	seawater + 3.8 g motor oil	750 ml liquid	intimate mixing	6 min	21°C	pressure change	H_2 presumed	85% H_2 generated in 1 min
exp. 12	LiH, 15 g	fine polyxtal powder	N_2 pressurized to 47.9 kPa	seawater + 8.3 g motor oil + detergent	750 ml liquid	intimate mixing	6 min	21°C	pressure change	H_2 presumed	100% H_2 generated in 1 min
exp. 13	LiH, 15 g	fine polyxtal powder	N_2 pressurized to 47.9 kPa	seawater + 7.5 g paint thinner	750 ml liquid	intimate mixing	6 min	21°C	pressure change	H_2 presumed	110% H_2 generated in 1 min
exp. 14	LiH, 30 g	coarse polyxtal powder	N_2 pressurized to 47.9 kPa	seawater + 15 g hydraulic oil	750 ml liquid	intimate mixing	6 min	21°C	pressure change	H_2 presumed	43% H_2 generated in 1 min
exp. 15	LiH, 15 g	fine polyxtal powder	N_2 pressurized to 47.9 kPa	seawater + 7.5 g diesel oil	750 ml liquid	intimate mixing	6 min	21°C	pressure change	H_2 presumed	127% H_2 generated in 1 min
exp. 16	LiH, 15 g	fine polyxtal powder	N_2 pressurized to 47.9 kPa	seawater + 7.5 g hydraulic oil	750 ml liquid	intimate mixing	6 min	21°C	pressure change	H_2 presumed	101% H_2 generated in 1 min
exp. 17	LiH, 15 g	fine polyxtal powder	n/m	seawater + 7.5 g DC200	750 ml liquid	intimate mixing	6 min	21°C	pressure change	H_2 presumed	
exp. 18	LiH, 15 g	fine polyxtal powder	N_2 pressurized to 47.9 kPa	seawater + 7.5 g DC200	750 ml liquid	intimate mixing	6 min	21°C	pressure change	H_2 presumed	101% H_2 generated in 1 min
exp. 19	LiH, 15 g	50 w%/50 w% coarse polyxtal powder	n/m	seawater + 6.0 g DC200	750 ml liquid	intimate mixing	6 min	21°C	pressure change	H_2 presumed	
exp. 20	LiH, 15 g	fine polyxtal powder	N_2 pressurized to 47.9 kPa	seawater + 7.5 g hydraulic oil	750 ml liquid	intimate mixing	6 min	21°C	pressure change	H_2 presumed	
exp. 21	LiH, 30 g	50 w%/50 w% coarse polyxtal powder	N_2 pressurized to 7.18 kPa	seawater + 7.5 g paint thinner	750 ml liquid	intimate mixing	6 min	21°C	pressure change	H_2 presumed	92% H_2 generated in 1 min
exp. 22	LiH, 30 g	fine polyxtal powder	N_2 pressurized to 7.90 kPa	seawater + 10 g paint thinner	750 ml liquid	intimate mixing	6 min	21°C	pressure change	H_2 presumed	110% H_2 generated in 1 min
Dinh, Balooch, Cecala, Leckey; 2001											
exp. 1	LiD	single xtal {100}	air, ambient pressure	from air	1783*	continuous	1800 min	27°C, method n/m	SEM	none	18-20 μm in 1800 min
exp. 2	LiD	single xtal {100}	air, ambient pressure	from air	1783* assuming H_2O temp @ 27°C	continuous	1800 min	66°C, method n/m	SEM	none	3-5 μm in 1800 min
Holcombe, 1972											
exp. 1, st. 1 st. 3, st. 5, st. 7.	LiH	polyxtal pellet	air	from air	317*	continuous	42000 min (in 4 steps alternating with Ar)	n/m, assume RT	–	–	
exp. 1, st. 2 st. 4, st. 6, st. 8.			Ar	–	–	continuous	3960 min (in 4 steps alternating with air)	n/m, assume RT	gravimetry, SEM	none	$W = 14.2 + 0.549t$
exp. 2, st. 1 st. 3, st. 5, st. 7.	LiH	polyxtal pellet	air	from air	317*	continuous	42000 min (in 4 steps alternating with Ar)	n/m, assume RT	–	–	
exp. 2, st. 2 st. 4, st. 6, st. 8.			CO_2	–	–	continuous	3960 min (in 4 steps alternating with air)	n/m, assume RT	gravimetry, SEM	none	$W = 14.0 + 0.446t$
exp. 3, st. 1	LiH	polyxtal pellet	0.5% F in N_2 (no unit),0.5 atm	–	–	single dose	15 min	n/m, assume RT	–		
st. 2			air	from air	317*	continuous	21300 min	n/m, assume RT	gravimetry	none	$W = 18.2 + 0.386t$

W = weight (mg/cm^2)
t = time (hours)

exp. #, step #	SAMPLE MATERIAL	SAMPLE FORM	EXPOSURE ENVIRONMENT	H_2O PURITY	H_2O CONTENT (Pa)	EXPOSURE PROCESS	EXPOSURE TIME	EXPOSURE TEMPERATURE	ANALYSIS TECHNIQUES	PRODUCTS IDENTIFIED	KINETIC EXPRESSIONS
Holcombe, Powell; 1973											
exp. 1	LiH	single xtal, {100}	air	from air	1268*	continuous	~6 months	RT	XRD, SEM	trace LiOH•H_2O, LiOH, LiH	
exp. 2, st. 1	LiH	single xtal, {100}	vacuum	–	–	–	–	"heated"	–		
st. 2			air	from air	1268*	continuous	~6 months	RT	XRD, SEM	Li_2CO_3, LiOH, LiH,	
st. 3			vacuum	–	–	continuous	20160 min	200°C	XRD, SEM	Li_2CO_3/LiOH/Li_2O/LiH (bulk)	
Kong, Foulkes, Kirk, Hinatsu; 1999											
exp. 1	LiH	polyxtal powder	gas n/m, ~1 atm	deionized	liquid "drops"	direct contact, 1 drop/15 sec	up to ~400 min	25°C; then rxn generated heat	pressure change	H_2 presumed	H_2 = 1.4x10^{-4} mol/g•s
exp. 2	LiH	polyxtal powder	gas n/m, ~1 atm	deionized	stoichiometric excess H_2O (g)	continuous	up to ~400 min	25°C; then rxn generated heat	pressure change	H_2 presumed	H_2 = 2.8x10^{-5} mole/g•s
Kong, Foulkes, Kirk, Hinatsu; 2003											
exp. 1	LiH	polyxtal powder	n/m	n/m, sometimes KOH added	700	continuous	up to ~400 min	0-~70°C, method unclear	pressure change	H_2 presumed	H_2 =~0.050 @ 0°C, ~0.050 @ ~67°C mol/kg•s
exp. 2		polyxtal powder	n/m	n/m, sometimes KOH added	1400	continuous	up to ~400 min	~15-40°C, method unclear	pressure change	H_2 presumed	H_2 =~0.014 @ ~12°C, ~0.018 @ ~40°C mol/kg•s
exp. 3		polyxtal powder	n/m	n/m, sometimes KOH added	3000	continuous	up to ~400 min	~25-50°C, method unclear	pressure change	H_2 presumed	H_2 =~0.029 @ ~25°C, ~0.033 @ ~50°C mol/kg•s
exp. 4		polyxtal powder	n/m	n/m, sometimes KOH added	6100	continuous	up to ~400 min	~35-50°C, method unclear	pressure change	H_2 presumed	H_2 =~0.045 @ ~35°C, ~0.049 @ ~50°C mol/kg•s
exp. 5		polyxtal powder	n/m	n/m, sometimes KOH added	11500	continuous	up to ~400 min	~50°C, method unclear	pressure change	H_2 presumed	H_2 =~0.085 @ ~50°C mol/kg•s
Leckey; 1996											
exp. 1	LiH	polyxtal pellet	n/m, assume air, & atm pressure	n/m	1800 ml, liquid	intimate mixing	at least 1400 min	34-36°C, solution temp controlled	solution conductivity	LiOH, Li^+, OH^- all presumed	
Machin, Tompkins; 1966											
exp. 1	LiH, 1-2 g	polyxtal powder	vacuum	purified	25	in 3 doses	up to ~180 min	0°C, method n/m	gravimetry, pressure change, gas composition	Li_2O to 1 monolayer H_2O, LiOH at greater H_2O, deduced	
exp. 2	LiH, 1-2 g	polyxtal powder	vacuum	purified	987	in 12 doses	up to ~180 min	48.4°C, method n/m	gravimetry, pressure change, gas composition	Li_2O to 1 monolayer H_2O, LiOH at greater H_2O, deduced	
exp. 3	LiH, 1-2 g	polyxtal powder	vacuum	purified	30	in 3 doses	up to ~180 min	48.4°C, method n/m	gravimetry, pressure change, gas composition	Li_2O to 1 monolayer H_2O, LiOH at greater H_2O, deduced	
exp. 4	LiH, 1-2 g	polyxtal powder	vacuum	purified	883	in 11 doses	up to ~180 min	70.0°C, method n/m	gravimetry, pressure change, gas composition	Li_2O to 1 monolayer H_2O, LiOH at greater H_2O, deduced	
exp. 5	LiH, 1-2 g	polyxtal powder	vacuum	purified	21	in 3 doses	up to ~180 min	70.0°C, method n/m	gravimetry, pressure change, gas composition	Li_2O to 1 monolayer H_2O, LiOH at greater H_2O, deduced	
exp. 6	LiH, 1-2 g	polyxtal powder	vacuum	purified	103	in 5 doses	up to ~180 min	93.8°C, method n/m	gravimetry, pressure change, gas composition	Li_2O to 1 monolayer H_2O, LiOH at greater H_2O, deduced	
exp. 7	LiH, 1-2 g	polyxtal powder	vacuum	purified	150	in 6 doses	up to ~180 min	121.0°C, method n/m	gravimetry, pressure change, gas composition	Li_2O to 1 monolayer H_2O, LiOH at greater H_2O, deduced	$D=\frac{1}{t}\ln\left(\frac{a}{a-x}\right)-\frac{Cx}{t}$
McLaughlin, Cristy; 1974											
exp. 1	LiD	single xtal	Ar, glovebox pressure	n/m	0.2666°	continuous	720 sec	22°C	SIMS	indistinct layers, O and H at surface	
exp. 2	LiD	single xtal	air, atm press.	from air	1718*	continuous	35 sec	22°C	SIMS	LiOH/Li_2O/LiD (bulk)	
exp. 3	LiD	single xtal	air, atm press.	from air	2036*	continuous	20 sec	22°C	SIMS	LiOH/Li_2O/LiD (bulk)	
Myers; 1974											
exp. 1	LiH	single xtal {100}	air, atm pressure	from air	1405*	continuous	~15 min	23°C	RBS	LiOH/LiH (bulk)	
exp. 2	LiH	single xtal {100}	vacuum	purified	266	continuous	300-1800 min	23°C	RBS	LiOH/LiH (bulk)	

$$f_s = 1 - \sum_{n=1}^{\infty} \frac{4L^2 \exp\left(-\beta_n^2 Dt / r_b^2\right)}{\beta_n^2(\beta_n^2 + L^2)}$$

f_s = fractional conversion of a hydride slab
D = diffusivity of H_2O through
r_b = radius of the hydride bed
$L = r_b \alpha D$
r_b = radius of the hydride bed
α = average penetration rate of the water vapor
β = constants
t = time

$$\frac{dc}{dt} = \alpha k A(t)\left(1 - \frac{\gamma_s(c)t}{\gamma_{s,s}} \times \frac{c}{c_s}\right)$$

ρ = mass density of solid LiH
M_w = molecular weight of LiH
V = volume of LiH
c = concentration
t = time
k = rate constant for LiH reacted in terms of depth per time
$A(t)$ = surface area of of LiH as a function of time
$\gamma_s(c)$ = activity coefficient of LiOH in solution at any time (concentration dependent)
$\gamma_{s,s}$ = activity coefficient of LiOH in saturated aqueous solution

x = H_2 pressure after time, t (torr)
a = final H_2 pressure (torr)
t = time (minutes)
C and D are constants in any particular run

exp. #, step #	SAMPLE MATERIAL	SAMPLE FORM	EXPOSURE ENVIRONMENT	H_2O PURITY	H_2O CONTENT (Pa)	EXPOSURE PROCESS	EXPOSURE TIME	EXPOSURE TEMPERATURE	ANALYSIS TECHNIQUES	PRODUCTS IDENTIFIED	KINETIC EXPRESSIONS
Phillips; 1995											
exp. 1	LiH, 15 g	polyxtal powder	Ar	n/m	34800 Pa (149 μmol) doses	~1 dose/hour	at least 720 min	232°C, LiH & H_2O heated	calorimetry, H_2 production	LiOH, Li_2O, LiH, H_2	
exp. 2	LiH, 15 g	polyxtal powder	Ar	n/m	40516 Pa (149 μmol) doses	~1 dose/hour	at least 720 min	315°C, LiH & H_2O heated	calorimetry, H_2 production	LiOH, Li_2O, LiH, H_2	
Pitcher; 1997											
exp. 1	LiH, 1 g	polyxtal pellet	Ar, 0.25 MPa	distilled	1 ml/min liquid	continuous flow, direct contact	30-90 min	22°C; rxn zone ~90°C	pressure change	H_2 presumed	3.75 mmol/min H_2 produced
exp. 2	LiH, 1 g	polyxtal pellet	Ar, 0.25 MPa	distilled	2 ml/min liquid	continuous flow, direct contact	30-90 min	n22°C; rxn zone ~90°C	pressure change	H_2 presumed	6.60 mmol/min H_2 produced
exp. 3	LiH, 1 g	polyxtal pellet	Ar, 0.50 MPa	distilled	1 ml/min liquid	continuous flow, direct contact	30-90 min	22°C; rxn zone ~90°C	pressure change	H_2 presumed	3.40 mmol/min H_2 produced
exp. 4	LiH, 1 g	polyxtal pellet	Ar, 0.50 MPa	distilled	2 ml/min liquid	continuous flow, direct contact	30-90 min	22°C; rxn zone ~90°C	pressure change	H_2 presumed	5.89 mmol/min H_2 produced
exp. 5	LiH, 1 g	polyxtal pellet	Ar, 1.0 MPa	distilled	1 ml/min liquid	continuous flow, direct contact	30-90 min	22°C; rxn zone ~90°C	pressure change	H_2 presumed	2.57 mmol/min H_2 produced
exp. 6	LiH, 1 g	polyxtal pellet	Ar, 1.0 MPa	distilled	2 ml/min liquid	continuous flow, direct contact	30-90 min	22°C; rxn zone ~90°C	pressure change	H_2 presumed	4.96 mmol/min H_2 produced
exp. 7	LiH, 1 g	polyxtal pellet	Ar, 1.5 MPa	distilled	1 ml/min liquid	continuous flow, direct contact	30-90 min	22°C; rxn zone ~90°C	pressure change	H_2 presumed	2.75 mmol/min H_2 produced
exp. 8	LiH, 1 g	polyxtal pellet	Ar, 1.5 MPa	distilled	2 ml/min liquid	continuous flow, direct contact	30-90 min	22°C; rxn zone ~90°C	pressure change	H_2 presumed	4.60 mmol/min H_2 produced
exp. 9	LiH, 6.5 g	polyxtal pellet	Ar, 0.50 MPa	distilled	2 ml/min liquid	continuous flow, direct contact	30-90 min	22°C; rxn zone ~90°C	pressure change	H_2 presumed	7.55 mmol/min H_2 produced
exp. 10	LiH, 6.5 g	polyxtal pellet	Ar, 0.50 MPa	distilled	4 ml/min liquid	continuous flow, direct contact	30-90 min	22°C; rxn zone ~90°C	pressure change	H_2 presumed	15.0 mmol/min H_2 produced
exp. 11	LiH, 6.5 g	polyxtal pellet	Ar, 1.0 MPa	distilled	2 ml/min liquid	continuous flow, direct contact	30-90 min	22°C; rxn zone ~90°C	pressure change	H_2 presumed	6.85 mmol/min H_2 produced
exp. 12	LiH, 1 g	polyxtal pellet	Ar, 0.50 MPa	seawater	1 ml/min liquid	continuous flow, direct contact	30-90 min	22°C; rxn zone ~90°C	pressure change	H_2 presumed	3.00 mmol/min H_2 produced
exp. 13	LiH, 1 g	polyxtal pellet	Ar, 0.50 MPa	seawater	2 ml/min liquid	continuous flow, direct contact	30-90 min	22°C; rxn zone ~90°C	pressure change	H_2 presumed	4.93 mmol/min H_2 produced
Powell, Milosevic, Lucania, Harrick; 1992											
exp. 1	LiH	polyxtal pellet	Ar @ glovebox pressure	n/m	7°	continuous	~30000 min	n/m, assume RT	IR, gravimetry	LiOH, LiH	82 mmole/minute final slope LiOH growth
exp. 2	LiD	polyxtal pellet	air	from air	317*	continuous	several days	n/m, assume RT	IR, gravimetry	LiOD, LiD, Li_2CO_3	parabolic, then linear
Rozenband; 1975											
exp. 1	LiH	polyxtal pellet	n/m, assume air, atm pressure	n/m	large, container of liquid	intimate mixing	up to 2 sec	~25-35°C, LiH temp measured	solution temperature	none	~2.5°C/sec
exp. 2	LiH	polyxtal pellet	n/m, assume air, atm pressure	with 10% (no unit) ethanol	large, container of liquid	intimate mixing	up to 2 sec	~25-35°C, LiH temp measured	solution temperature	none	$q = 1.4 \times 10^{19} C_0 \exp\left(-\frac{6{,}210}{RT}\right)$
exp. 3	LiH	polyxtal pellet	n/m, assume air, atm pressure	with 20% (no unit) ethanol	large, container of liquid	intimate mixing	up to 2 sec	~25-35°C, LiH temp measured	solution temperature	none	q = heat generated, J/cm²•sec
exp. 4	LiH	polyxtal pellet	n/m, assume air, atm pressure	with 30% (no unit) ethanol	large, container of liquid	intimate mixing	up to 2 sec	~25-35°C, LiH temp measured	solution temperature	none	C_0 = volumetric coefficient of oxidant R = gas constant, J/mol•K T = temperature, K
Smyrl, Fuller, Powell; 1983											
exp. 1	LiH	polyxtal powder	vacuum	n/m	2500	multiple doses	3300 min	26°C	IR	LiOH•H_2O, LiOH, LiH	

Table 4
Summary of experiments for reactions between LiH hydrolysis products

exp. #	step #	SAMPLE MATERIAL	SAMPLE FORM	EXPOSURE ENVIRONMENT	CHEMICAL EXPOSURE	EXPOSURE CHEMICAL CONTENT	EXPOSURE TEMPERATURE	EXPOSURE TIME	EXPOSURE PROCESS	ANALYSIS TECHNIQUES		PRODUCTS IDENTIFIED
* = converted from relative humidity value using HCON software from General Eastern Instruments. The following values were used: 25°C (ambient) or applicable temperature value, 101.3 kPa (ambient) or applicable pressure value, and 29 g/mole (air) or applicable molecular weight value; ° = converted from ppm value in literature with no mention of unit, ppmv is assumed; n/m = not mentioned in the literature, RT = room temp.												
–A note on H_2O content units: Different authors have reported H_2O contents in different units. We have attempted to convert all H_2O contents to the same unit for comparisons. The reviewers would prefer units of mole, however literature authors have frequently reported H_2O contents in pressure units without providing additional information for conversions to moles. Therefore, we present H_2O contents in pressure units as that is the most accessible unit for comparison.												
Broughton, 2001												
exp. 1		LiH	n/m	n/m, assume vacuum	–	–	RT to 500°C	n/m	continuous	TPD	H_2	
exp. 2		LiH	polyxtal pellet	vacuum	–	–	30°C, 60°C, 90°C	~1116000 min (~775 days)	continuous with temp changes	gas volume	H_2 presumed	($\sim 1\times10^{-6}$ mol H_2/mol LiH)/day
Dinh, Balooch, Cecala, Leckey; 2001												
exp. 1		LiOH	as prepared powder	–	–	–	RT to ≥525°C	–	H_2O	TPD, SEM	H_2O	$\alpha(t) = 1 - \left\{1 - \left[\frac{\nu}{3} t e^{-(E/RT)}\right]\right\}^3$
exp. 2, st. 1		LiD	single xtal {100}	air	H_2O, from air	941-1268 Pa* H_2O	n/m, assume RT	8 min		SEM		
st. 2				vacuum	–	–	RT to ~700°C	–	H_2	TPD	H_2O	$\alpha(t) = 1 - \exp\left[-t\nu e^{-(E/RT)}\right]$
exp. 3, st. 1		LiD	single xtal {100}	air	H_2O, from air	941-1268 Pa* H_2O	n/m, assume RT	120 min				
st. 2				vacuum	–	–	RT to ~700°C	–	continuous	TPD	H_2O, H_2, D_2, HD	
exp. 4, st. 1		LiD	single xtal {100}	vacuum	–	–	RT to ≥450°C	2880 min at 230°C	heat, then cool	TPD	H_2O	$\alpha(t) = 1 - \left\{\left[1 - \frac{\kappa}{r}\left(\frac{T - T_0}{\beta}\right)\right]^2\left[1 - \frac{\kappa}{Z}\left(\frac{T - T_0}{\beta}\right)\right]\right\}^3$
st. 2				n/m	H_2O, purity n/m	4.0 Pa°	RT	240 min	continuous			
st. 3				vacuum	–	–	RT to ≥550°C	2880 min at 230°C	heat, then cool	TPD	H_2O	
st. 4				n/m	H_2O, purity n/m	40 Pa°	RT	192 min	continuous			
st. 5				vacuum	–	–	RT to ≥ 550°C	2880 min at 230°C	heat, then cool	TPD	H_2O	
st. 6				n/m	H_2O, purity n/m	79 Pa°	RT	1200 min	continuous			
st. 7				vacuum	–	–	RT to ≥550°C	2880 min at 230°C	heat, then cool	TPD	H_2O	
Dinh, Balooch, Cecala, Leckey; 2003												
exp. 1		LiOH	as prepared polyxtal powder	–	vacuum	–	RT to ~750°C	–	continuous	TPD	H_2O; presumed that LiOH converted to Li_2O	$\alpha(t) = 1 - \left\{1 - \left[\frac{\nu}{3} t e^{-(E/RT)}\right]\right\}^3$
exp. 2, st. 1		LiOH	polyxtal powder	vacuum	–	–	RT to ~750°C	–	continuous	TPD	H_2O; presumed that LiOH converted to Li_2O	
st. 2			polyxtal powder	n/m	H_2O	~20 Pa H_2O	RT	30 min	continuous		~3% Li_2O converted to LiOH (from subsequent TPD)	
st. 3			polyxtal powder	–	–	–	RT to ~750°C	–	continuous	TPD	H_2O; presumed that LiOH converted to Li_2O	
st. 4			polyxtal powder	n/m	H_2O	~2.7 Pa H_2O	RT	30 min	continuous		~1.5% Li_2O converted to LiOH (from subsequent TPD)	
st. 5			polyxtal powder	–	–	–	RT to ~750°C	–	continuous	TPD	H_2O; presumed that LiOH converted to Li_2O	$\alpha(t) = 1 - \exp\left[-t\nu e^{-(E/RT)}\right]$
st. 6			polyxtal powder	n/m	H_2O	~0.8 Pa H_2O	RT	30 min	continuous		~0.1% Li_2O converted to LiOH (from subsequent TPD)	
st. 7			polyxtal powder	–	–	–	RT to ~750°C	–	continuous	TPD	H_2O; presumed that LiOH converted to Li_2O	
exp. 3, st. 1		LiD	polyxtal powder	air, ambient pressure	H_2O, from air	1267 Pa* H_2O	RT	up to 338 min	continuous	XRD	LiD, LiOH, LiOH•H_2O	
st. 2				–	–	–	RT to ~750°C	n/m	continuous	TPD	H_2O, H_2, HD, D_2	$D = 4.1467\times10^{-16}\exp\left(\frac{-44929}{8.314T}\right)$
Frazer; 1958												
exp. 1		LiH with 4.19 w% LiOH	polyxtal pellet	vacuum	–	–	400°C	~240-360 min	continuous	pressure change	H_2 presumed	
exp. 2		LiH with 3.82 w% LiOH	polyxtal pellet	vacuum	–	–	400°C	~240-360 min	continuous	pressure change	H_2 presumed	
exp. 3		LiH with .0944 w% LiOH	polyxtal pellet	vacuum	–	–	400°C	~240-360 min	continuous	pressure change	H_2 presumed	
Furuyama, Ito, Dohi, Taniike, Kitamura; 2003												
exp. 1		LiOH, LiOD	polyxtal thin film	vacuum	–	–	RT- ~800°C	–	continuous	TPD	HDO, D_2O, D_2	
exp. 2		LiH	n/m, assume polyxtal powder	vacuum	–	–	RT- ~850°C	–	continuous	TPD	H_2, H_2O	
exp. 3		LiOH	n/m, assume polyxtal powder	vacuum	–	–	RT- ~850°C	–	continuous	TPD	H_2, H_2O	

exp. 1
for H_2O from LiOH•H_2O & for LiOH to Li_2O conv.:
α = reacted fraction, t = time
R = constant, T = temperature
$\nu = 6.9\times10^9$ s^{-1},
E = 136 kJ/mole

exp. 2
for H_2O from LiOH•H_2O & for LiOH to Li_2O conversion
α = reacted fraction, t = time
R = constant, T = temperature
$\nu = 10^5$–10^7 s^{-1},
E = 48, 67 kJ/mole

exp. 3
for LiOH to Li_2O conversion:
α = reacted fraction, t = time, T = temperature
r = average radius of hydrolysis structure = 45 nm
Z = average height of hydrolysis structure = 45 nm
β = heating rate = 0.46 k/s,
$\kappa = \kappa_0 e^{-(E/RT)}$, κ_0 = 5.4–2.4 nm/s,
E = 122-129 kJ/mol, R = gas constant

exp. 4
for LiOH to Li_2O conversion:
E = 83-102 kJ/mole

for LiOH to Li_2O conversion:
α = reacted fraction, t = time
R = constant, T = temperature
exp. 1
$\nu = 10^6$–10^9 s^{-1}, E = 115-142 kJ/mol
exp. 2, step 2-3
$\nu = 10^6$–10^7 s^{-1}, E = 99-108 kJ/mol
exp. 2, step 4-5
$\nu = 10^6$–10^7 s^{-1}, E = 89-96 kJ/mol

for LiOH to Li_2O conversion:
α = reacted fraction, t = time
R = constant, T = temperature
exp. 2, step 6-7
$\nu = 6.9\times10^9$ s^{-1},
E = 86-92 kJ/mol
exp. 3
$\nu = 10^5$–10^7 s^{-1},
E = 86-92 kJ/mol

exp. 3
for LiOH+LiH→Li_2O+H_2:
D = diffusion coefficient of LiOH in Li_2O
T = temperature

exp. #, step #	SAMPLE MATERIAL	SAMPLE FORM	EXPOSURE ENVIRONMENT	CHEMICAL EXPOSURE	EXPOSURE CHEMICAL CONTENT	EXPOSURE TEMPERATURE	EXPOSURE TIME	EXPOSURE PROCESS	ANALYSIS TECHNIQUES	PRODUCTS IDENTIFIED	KINETIC EXPRESSIONS
Kopasz, Ortiz-Villafuerte, Johnson; 1994											
exp. 1, st. 1	Li_2O with some LiOH	polyxtal powder	D_2, pressure n/m	D_2	100%	250°C	180-1440 min	flowing gas			
st. 2			Ar, pressure n/m	–	–	250-1000°C	–	flowing gas	TPD	TPD peak @~700°C, presumed desorption of OD^- from Li_2O	
exp. 2, st. 1	Li_2O with some LiOH	polyxtal powder	D_2, pressure n/m	D_2	100%	250°C	180-1440 min	flowing gas			
st. 2			Ar, pressure n/m	H_2	1 mol%	250-1000°C	–	flowing gas	TPD	TPD peak @~700°C, presumed desorption of OD^- from Li_2O; ~950°C peak had no ID	
exp. 3	Li_2O with some LiOH	polyxtal powder	Ar, pressure n/m	H_2 or D_2	1 mol%	100-400°C	–	flowing gas	IR	four OH^- species & four OD^- species, hydride species	
exp. 4, st. 1	Li_2O with some LiOH	polyxtal powder	Ar, pressure n/m	D_2	1 mol%	120°C	960 min	flowing gas	TPD with IR	OH^- species	
st. 2			Ar, pressure n/m	H_2	1 mol%	120-400°C	–	flowing gas	TPD with IR	OH^- species removed, replaced with hydride species	
Kudo; 1979											
exp. 1	LiOH	polyxtal powder	–	–	–	257-417°C	–	continuous	MS, IR, radiation levels	H_2O	$k_{H2O} = 1.8\times10^8$ exp(123500/RT); LiOH to Li_2O conversion; R=J/mol•K
exp. 2	LiOD	polyxtal powder	–	–	–	257-417°C	–	continuous	MS, IR, radiation levels	D_2O	$k_{D2O} = 1.7\times10^8$ exp(121400/RT); LiOH to Li_2O conversion; R=J/mol•K
exp. 3	LiOT	polyxtal powder	–	–	–	257-417°C	–	continuous	MS, IR, radiation levels	radioactive species	$k_{HTO} = 1.6\times10^7$ exp(128500/RT); LiOH to Li_2O conversion; R=J/mol•K
McIntyre; 1970											
exp. 1, st. 1	LiOH	polyxtal powder	Ar	–	–	200°C	–	flowing Ar	weight change, Li_2O and H_2 presumed		
st. 2	LiOH	polyxtal powder	vacuum	–	–	200-400°C	–	continuous	weight change, Li_2O and H_2 presumed		LiOH to Li_2O conversion
Myers; 1974											
exp. 1, st. 1	LiH	single xtal {100}	air, atm pressure	H_2O, from air	1584 Pa*	23°C	~15 min	continuous	RBS	LiOH/LiH (bulk)	
st. 2			vacuum	–	–	280°C	n/m	continuous	RBS	Li_2O/LiH (bulk)	
exp. 2, st. 1	LiH	single xtal {100}	vacuum	H_2O, distilled	200-267 Pa	23°C	n/m	single dose	RBS	LiOH/LiH (bulk)	
st. 2			vacuum	–	–	250°C	360 min	continuous	RBS	Li_2O/LiH (bulk)	linear;~5×10^{14}-5×10^{16} O atoms/cm²•s @ 200-280°C LiOH to Li_2O conversion
exp. 3, st. 1	LiH	single xtal {100}	vacuum	H_2O, distilled	200-267 Pa	23°C	n/m	single dose	RBS	LiOH/LiH (bulk)	
st. 2			vacuum	–	–	280°C	360 min	continuous	RBS	Li_2O/LiH (bulk)	linear;~5×10^{14}-5×10^{16} O atoms/cm²•s @ 200-280°C LiOH to Li_2O conversion
Newton, Challenger, Holley, Alei, Head, Zalkin, Ready, Florin, White, Shlaer; 1954											
exp. 1, st. 1	LiH	polyxtal pellet	n/m, assume air, atm pressure	H_2O, from air	348	n/m, assume RT	n/m	continuous	weight gain, pressure change	LiOH, H_2 presumed	
st. 2			n/m	–	–	262-269°C	45 hours	continuous	pressure change	H_2 presumed	
exp. 2	50 mole% LiH/50 mole% LiOH	polyxtal pellet	n/m	–	–	240°C	n/m	continuous	pressure change	H_2 presumed	3.25×10^{-2} mmoles/hr; LiOH to Li_2O conversion
exp. 3	50 mole% LiH/50 mole% LiOH	polyxtal pellet	n/m	–	–	150°C	n/m	continuous	pressure change	H_2 presumed	1×10^{-3} mmoles/hr; LiOH to Li_2O conversion
Nishikawa, Kawamura, Munakata, Matsumoto; 1990											
exp. 1, st. 1	Li_2O	polyxtal powder	He, atm pressure	–	–	700°C	12+ hours	flowing, 400 mL/min			
st. 2			He, atm pressure	H_2	200-30,000 ppm (no unit)	500-700°C	≥800 min	flowing, 400 mL/min	hygrometry, gas chromatography	H_2, H_2O	
Popescu, Alexandrescu, Mihailescu, Morjam Pascu; 1988											
exp. 1	LiOH•H_2O	polyxtal powder	air	same as exp. environment	100%	RT-1000°C	–	–	DTA, TGA		
Stecura; 1973											
exp. 1	LiOH	polyxtal powder	vacuum	–	–	640-730°C	48 h	continuous	XRD	Li_2O_2	

$1-\alpha^{\frac{1}{3}} = 1-\frac{kt}{R}$ α = reacted fraction, k = rate constant, R = particle radius

Li$_2$O growth

$S = \gamma P_{H2O}(2\pi k_B mT)^{-\frac{1}{2}}$ S = adsorption rate of H_2O molecules, γ = fraction of H_2O retained molecules, P_{H2O} = H_2O pressure, k_B = Boltzmann constant, m = mass of H_2O molecule, T = temperature

$\ln(1-\alpha)^n = -\frac{E}{RT} + \ln\frac{A}{b} + L$ α = reacted fraction, T = temperature, K, b = heating rate, R = gas constant, kJ/mol, L = correction factor

for LiOH•H_2O → LiOH + H_2O:
E = activation energy, = 63 kJ/mol
A = preexponential factor, 10^7 1/s
reaction order = 1

for LiOH to Li_2O conversion:
E = activation energy, = 101 kJ/mol
A = preexponential factor, 10^7 1/s

accessible unit for comparison. Many of the original figures have been modified to show the same temperature, pressure, or other units, however, the reader should note that time units were not modified and that data are often displayed in different ways.

3.1. LiH reactions with low H_2O concentrations

One researcher, Broughton [15], completed computer simulations of reactions between LiH and H_2O. Force field calculations, based on molecular mechanics, indicated that half coverage of a LiH surface with H_2O led to a physisorbed complex with maximum stability which can then chemically react. Greater coverage with H_2O did not improve reactivity. This result was confirmed by quantum mechanical calculations, based on density functional theory. A potential energy scan of the adsorption of H_2O onto a LiH cluster predicted that the reaction should proceed without any barrier; however, Broughton indicated that this calculation was preliminary and needed improvements.

In 1966, Machin and Tompkins [12] studied LiH hydrolysis by reacting polycrystalline LiH particles with consecutive doses of high purity H_2O vapor in vacuum. The H_2O doses ranged from 21 to 987 Pa at 0 to 121 °C. Weight, pressure, and gas composition were all measured, as well as surface area of the LiH particles. The researchers concluded that the size of the H_2O dose determined the identity of the hydrolysis product formed; specifically a dose of up to one monolayer of H_2O produced Li_2O, while a larger dose of more than one monolayer produced only LiOH (H_2O values were specified here in 'layer' units because LiH particles with varying surface areas were used). LiOH was produced at larger doses, regardless of whether Li_2O or LiOH had previously formed. Machin and Tompkins theorized that Li_2O can take two forms: either α, which readily reacts with H_2O, or β, which forms upon annealing (restructuring) and does not react as easily with H_2O. The α form was suggested to be an intermediary product which then reacted with H_2O to form LiOH. Li_2O and LiOH were thought to not exist simultaneously (as suggested in Fig. 1), as the amount of Li_2O in these cases was termed 'negligible.' However, the researchers did not analyze samples for an Li_2O layer between LiH and LiOH. An angstrom-scale Li_2O layer could be consistent with such a small quantity, and in fact, fits well with the Machin and Tompkins (as well as other researchers [13,14]) suggestion that Li_2O is a precursor to formation of LiOH.

Phillips et al. [13] studied high-temperature hydrolysis in which polycrystalline LiH particles in 15 g quantities was reacted with 149-μmol (34 800 Pa at 232 °C or 40 516 Pa at 315 °C) doses of H_2O vapor added approximately every hour to an Ar gas flow at 93 mL/min. The H_2O vapor and LiH were both heated to either 232 °C or 315 °C. Calorimetry and H_2 production were used to monitor the reaction. The stoichiometric coefficients for reactant and product compounds, as well as heat of reaction values, were determined under continued H_2O dosing. Li_2O was initially the prevalent product, while continued dosing produced primarily LiOH. Phillips et al. identified that these results gave further evidence for the oxide first reaction mechanism, Rns. R3 and R4, for LiH hydrolysis at high temperatures. A further result was a delay in detection of H_2 after H_2O dosing; a similar delay was observed by Machin and Tompkins [12] and Balooch et al. [16]. Phillips interpreted the H_2 delay to result from diffusion of H_2 through an growing LiOH surface layer.

3.2. LiH reactions with high H_2O concentrations

A number of researchers have used hydrogen isotopes in their studies of lithium hydride hydrolysis to trace the source of hydrogen in the reaction products. By using either LiD with H_2O or LiH with D_2O as reactants and then quantifying the amount of D in the products, one can gain a better understanding of the reaction mechanisms.

Beutler et al. [35] reacted LiH particles with liquid D_2O (quantity unknown) in vacuum at an unspecified temperature (presumably RT). The resulting hydrogen gas was analyzed for isotopic identity and quantity using ultraviolet absorption measurements. The intensity ratio of HD to H_2 or D_2 was 4:1. The authors concluded that a D atom from D_2O replaces an H atom in LiH during hydrolysis. Therefore, $LiH + D_2O \rightarrow LiOD + HD$, or alternatively, $LiD + H_2O \rightarrow LiOH + HD$. They interpreted this result to mean that the reaction to form hydroxide from LiH is more fully expressed as

$$Li^+H^- + D^+(OD)^- \rightarrow LiOD + HD \quad \text{or}$$
$$Li^+D^- + H^+(OH)^- \rightarrow LiOH + HD \qquad \text{(R24)}$$

The breakdown of the LiH and H_2O into ionic reactants does not apply to the oxide forming reaction,

$2LiH + H_2O \rightarrow Li_2O + 2H_2$, in a straightforward manner. It would be necessary for the OH^- ion (of H_2O) to break apart so that O^{2-} is available to react with Li^+, i.e., $2(Li^+H^-) + H_2^+O^{2-} \rightarrow Li_2O + H_2$.

Holley [6] confirmed the result that LiD reacts with H_2O to form LiOH. The result was also quantified, with at least 96 at.% of the D converting to hydrogen gas (HD). Holley states that his result agrees quantitatively with the Beutler's [35]. Unfortunately, the experimental technique of Holley was not documented and it is not clear whether the product hydrogen gas was analyzed for isotopes, or whether the HD product was an assumption.

McLaughlin and Cristy [8] exposed single crystals of LiD to air at 22 °C and either 2059 Pa H_2O for 35 s or 2440 Pa H_2O for 20 s. The researchers used negative secondary ion-mass spectroscopy (SIMS) with sputtering to determine elemental contents and infer the identity of compounds. The results suggested a layered structure of LiOH/Li_2O/LiD (bulk); unfortunately layer thicknesses and rates could not be determined.

A similar study was later completed by Cristy [9] in which single crystal LiH was cleaved in an inert gas glovebox and then exposed to 347 Pa D_2O for 5 min (we assume at RT). SIMS determined that LiOD was present on the surface; D was not present beneath the LiOD layer. Li_2O was determined to exist beneath the LiOD layer, so that the layer structure was LiOD/Li_2O/LiH (bulk).

The findings from studies using isotopic variations of hydrogen are revealing. First, it is clear that the product hydroxide clearly derives its hydrogen atom from the water molecule. Secondly, studies in which LiD was reacted with H_2O found LiOH to be the hydroxide product, while studies in which LiH was reacted with D_2O found LiOD to be the hydroxide product. As detailed earlier, these results do not exclude the 'oxide first' reaction mechanism.

Holcombe and Powell [10] used X-ray diffraction (XRD) and scanning electron microscopy (SEM) to study hydrolysis reaction layers on the {1 0 0} faces of single crystal LiH. A first sample was exposed to air containing 1268 Pa of H_2O for ~259 200 min (~6 months), by placing the sample in a bottle with a wax paper lid. XRD identified LiH, LiOH, and $LiOH \cdot H_2O$ as products, with {1 1 0} being the preferred growth plane on the {1 0 0} LiH. The morphology for the LiOH was polycrystalline grains, ~1 μm. A second sample was given extensive vacuum treatments and then also placed in a wax paper covered bottle with air containing 1268 Pa of H_2O for ~259 200 min. XRD of this sample showed the presence of LiH, LiOH, and Li_2CO_3. After a 200 °C vacuum heat treatment, the hydrolyzed layers spalled; XRD and SEM of the LiH showed a 15-μm layer of Li_2O with a microstructure identical to the LiOH. SEM also showed that H_2O preferrentially attacked LiH at corners which led to cracking of the hydrolysis film and elimination of its passivating effect. No explanation was offered for the presence of carbonate on the vacuum treated sample only; however, one could speculate that the vacuum treated sample had a 'cleaner' surface (vacuum treatments have been found to remove H_2O from $LiOH \cdot H_2O$ [20]) that allowed it to form Li_2CO_3 when the sample was exposed to CO_2 in air. Alternatively, carbon could have been deposited on the vacuum treated sample as contaminant from the vacuum process, which subsequently formed Li_2CO_3 when exposed to air.

Infrared spectroscopy has also been used to determine hydrolysis products. In work by Smyrl et al. [7], LiH polycrystalline particles in vacuum were reacted with 2500 Pa H_2O over a 3300 min interval at 26 °C. After the pressure increased to ~10 kPa from H_2 production, the chamber was evacuated and re-exposed to H_2O vapor until pressure increases no longer occurred. Diffuse reflectance Fourier transform infrared spectroscopy (FTIR) showed that LiOH and $LiOH \cdot H_2O$ peaks grew while an LiH peak diminished after H_2O exposure. H_2O pressure reductions to 1300 Pa removed hydrate peaks while subsequent H_2O pressure increases to 2500 Pa reformed hydrate peaks. The hydroxyl peak was not removed by H_2O excursions below 1300 Pa. Buchanan and Bowen [36], showed similar results for product identification and reversibility, in which LiOH sample exposed to H_2O showed $LiOH \cdot H_2O$ peaks, and subsequent heating in vacuum removed hydrate peaks. Li_2O is not mentioned as a product in infrared (IR) studies; however, it may have been present below the resolution limit or deep within the sample. Powell et al. [28] showed that a polycrystalline LiD pellet exposed to 317 Pa H_2O in air for several days formed an Li_2CO_3 peak.

Myers used Rutherford backscattering spectroscopy (RBS) to study LiH hydrolysis reactions [11]. He found that exposing {1 0 0} single crystal LiH in a vacuum to either single doses of purified H_2O of 222–380 Pa at 23 °C, or to air containing 1584 Pa H_2O at RT and ambient pressure produced

a layer of LiOH at the surface of the LiH. Li_2O was not observed, but the experiment had a thickness resolution of ~15 keV, which would not have been sufficient to observe a very thin (<hundreds of angstroms) Li_2O layer. The sample which received the moist air exposure did not show C or N impurities; however, the RBS technique is not sufficiently sensitive to these impurities at the conditions of measurement to exclude these as reactants.

3.3. Reactions between LiH hydrolysis products

Newton et al. [6] prepared LiOH by exposing a pellet of polycrystalline LiH to air with a constant 348 Pa H_2O at (we assume) RT. He measured the weight gain to determine the amount of LiOH that formed. He then heated the LiOH sample to 269 °C for 2700 min while collecting the evolved gas. The evolved gas was not chemically identified, but rather presumed to be H_2. By comparing weight gain with pressure changes, he determined that 1 mole of LiOH produced 1 mole of H_2. This ratio satisfies the reaction $LiH + LiOH \rightarrow Li_2O + H_2$.

Using RBS, Myers found that heating LiOH on {100} single crystal LiH at 25–280 °C in vacuum converted the LiOH to Li_2O [11]. Myers concluded from concentration vs. depth profiles that the reaction to form Li_2O occurs on two fronts; the first front is at the sample surface where the reaction $2LiOH \rightarrow Li_2O + H_2O$ occurs, and the second front is at the LiOH/LiH interface where the reaction is $LiOH + LiH \rightarrow Li_2O + H_2$ (this is the sum of two reactions, $2LiOH \rightarrow Li_2O + H_2O$ and $2LiH + H_2O \rightarrow Li_2O + 2H_2$). The reaction fronts proposed by Myers are shown in Fig. 6.

Furuyama et al. [37] used TPD to study LiH reactions. TPD, in which samples were heated in vacuum at an unspecified rate, showed that a LiH 'standard' particles released H_2 at 100–350 °C and at 650 °C. The 100–350 °C TPD peak was not identified (it might be caused by a reaction from contaminant LiOH, i.e., $LiH + LiOH \rightarrow Li_2O + H_2$), but the 650 °C peak was identified by the authors as the disassociation of LiH. LiOH 'standard' particles showed an H_2O release at 440 °C, which was identified as the reaction $2LiOH \rightarrow Li_2O + H_2O$, as well as a very small release of H_2 at ~475 °C. A thin film was prepared that contained LiD, LiOD, and LiOH. TPD of this sample showed that D_2O and HDO releases (from the thin film) occurred at lower temperatures, 360 °C and 350 °C, respectively, when compared with the H_2O release at 440 °C from LiOH standard particles. Furuyama et al. suggested that the heavier isotopes may have a lower binding energy. A D_2 peak was observed at 510 °C. Furuyama et al. attributed this peak to the disassociation of LiD.

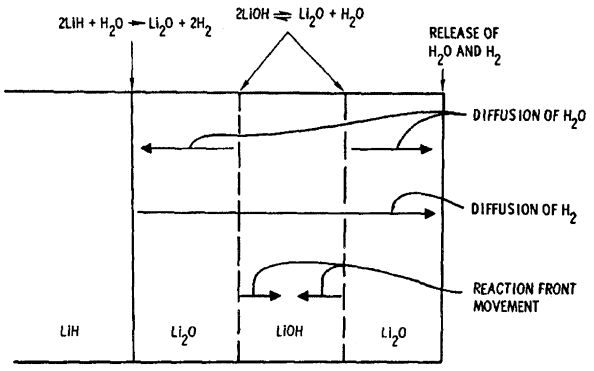

Fig. 6. Schematic of reactions to form Li_2O from LiOH on LiH at multiple interfaces, as proposed by Myers [11].

Dinh et al. [27] studied the decomposition of LiOH ($2LiOH \rightarrow Li_2O + H_2O$) of LiOH using TPD, in which samples were heated at rate of 0.46 °C/s. LiOH particles and hydrolyzed LiD single crystals (one exposed to air for 8 min, a second exposed for 120 min) were compared. H_2O was released from the briefly hydrolyzed LiD (i.e. containing a small quantity of LiOH) at a lower temperature (~250 °C) than for the LiOH particles (~330 °C). The longer hydrolyzed LiD sample (i.e. large quantity of LiOH), showed H_2O releases at two temperatures, which were similar to those of both the LiOH particles and the briefly hydrolyzed LiD. Dinh et al. attributed the lower temperature peak to the decomposition of imperfect or interface LiOH, while the higher temperature releases were attributed to the decomposition of standard LiOH. In a second paper by Dinh et al. [20], they again completed TPD (with a heating rate of 0.1 °C/s), comparing LiOH particles and small particles of hydroxide coated LiD. The results and conclusions were similar.

In further experiments [27], Dinh et al. alternately exposed single crystal LiD to first H_2O and then heat (during TPD analyses). Data showed that after exposure to a small amount of H_2O (to form LiOH), the subsequent TPD peak for H_2O was at a lower temperature than for sample exposed to a large amount of H_2O; this result was again interpreted to mean that LiOH formed at lower H_2O concentrations was more defective. Although absolute temperature values for TPD water peaks

differed between Dinh et al. and Furuyama et al. (likely in part because of different heating rates), both found that water was released from LiOH particles (or long-time hydrolyzed LiD) at higher temperatures than from LiOH resulting from (potentially defective) hydrolyzed LiD. The Dinh et al. experiment [27] further showed that the transformation between LiOH and Li_2O was reversible to some extent. The percentage of conversion from Li_2O to LiOH decreased with each iteration; however, it was not clear whether this was a result of a decreased capability for conversion, lower H_2O concentrations used in later H_2O exposures, or other reasons.

H_2, D_2, and HD were also released during TPD from hydrolyzed LiD [20,27]. The TPD spectrum showed peaks for these gases at temperatures at or slightly below H_2O releases. Dinh et al. considered these peaks to result from the reaction $LiOH + LiD \rightarrow Li_2O + dH_2 + eD_2 + fHD$ where $d + e + f = 1$. The presence of two oxide forming reactions during heating in hydrolyzed lithium hydride agrees with the reaction scheme proposed by Myers [11].

Finally, TPD completed by Dinh et al. on LiD samples exposed to H_2O showed a TPD H_2O peak upon heating that was far greater in intensity than the HDO or D_2O peak [20]. This is further evidence that LiOH (a lithium hydride hydrolysis product) obtains its hydrogen from water, rather than from lithium hydride: i.e. $LiD + H_2O \rightarrow LiOH + HD$ (or potentially H_2/D_2 if via the oxide first route) and then $2LiOH \rightarrow Li_2O + H_2O$.

Both TPD and gravimetric measurements were used by Broughton [15] to study reactions in heated polycrystalline LiH particles. The environments were not given, but were necessarily vacuum for the TPD measurements. Fig. 7 shows the data as a function of temperature; the heating rate was not specified. Broughton interpreted the H_2 peak at 500 °C to reflect the dissociation of LiH into Li metal and H_2 gas; this temperature is well below that reported by Furuyama for LiH (650 °C) [37] but similar to results for dissociation of LiD by both Furuyama (510 °C) and Dinh (~500 °C) [20,37]. Further H_2 peaks were observed at ~160 °C and 250 °C; the latter peak was the largest peak. Broughton considered the 250 °C peak to result from the reaction $LiH + LiOH \rightarrow Li_2O + H_2$ (LiOH is a contaminant in LiH). The origin of the 160 °C peak was less definitive, but Broughton suggested two possibilities. For both, the H_2 was a result of the reaction $LiH + H_2O \rightarrow LiOH + H_2$; the difference lay in the origin of the H_2O reactant. In the first possibility, H_2O evolved from inside the apparatus, while in the second, small amounts of H_2O were released from $LiOH \cdot H_2O$. Broughton considered the latter possibility to be more likely, as gravimetric data indicated a weight loss at 160 °C.

Popescu et al. [38] performed differential thermal analysis (DTA) and thermogravimetric analysis

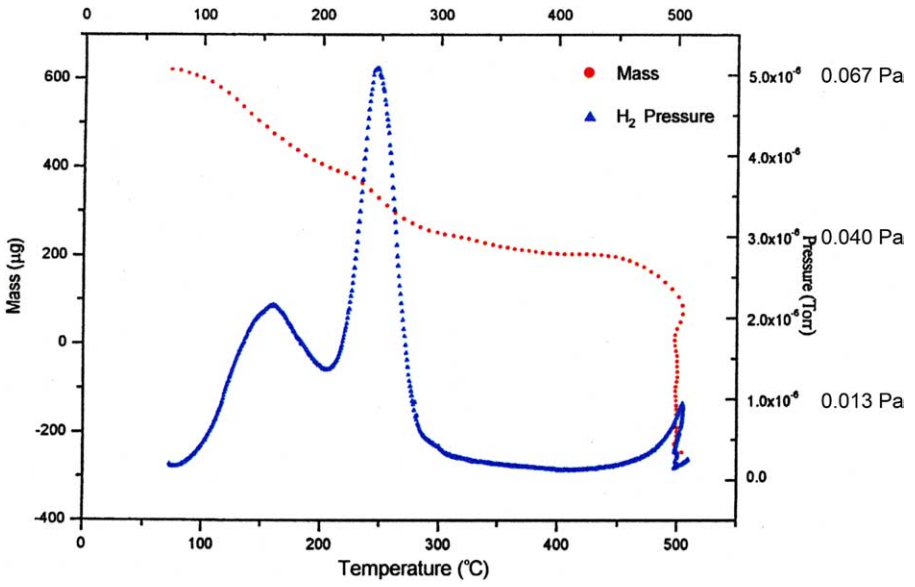

Fig. 7. Evolved H_2 and mass change for polycrystalline LiH particles as a function of temperature [15]. The present authors added SI units.

(TGA) on $LiOH \cdot H_2O$ polycrystalline particles in air. The heating rates were 10 °C/min. The DTA curve shows endothermic peaks at 110 °C, 415 °C (small), 462 °C, and 715 °C (very broad). Although individual DTA peaks were not interpreted by the authors, the 110 °C peak could be expected to be H_2O loss by the reaction $LiOH \cdot H_2O \rightarrow LiOH + H_2O$, and the 462 °C peak could be decomposition by the reaction $2LiOH \rightarrow Li_2O + H_2O$. The identity of the 415 °C and 715 °C peaks are not immediately obvious. The presence of two peaks (i.e. 415 °C and 462 °C) at the decomposition temperature range of LiOH has been observed previously [20,27,37], although most frequently when LiH was also present. The TGA data showed a weight loss onset at ~85 °C which was identified as H_2O loss from $LiOH \cdot H_2O$ and a weight loss onset at ~350 °C which was identified as H_2O loss from LiOH to form Li_2O. The weight loss regions were both broad, particularly the higher temperature region.

Kopasz et al. used TPD and diffuse reflectance IR to study the reaction of hydrogen with Li_2O [34]. For their IR studies, Li_2O samples were heated at various temperatures from 100 to 400 °C, while being purged with Ar + 0.1 mol% H_2 or Ar + 0.1 mol% D_2. Below 400 °C, four OH containing species (as well as four corresponding OD species) were observed; their presence depended on the temperature and hydrogen pressure of the system. The authors proposed that the four species were hydroxyls with coordination numbers of 2, 4, 6, and 8. Hydride peaks were also observed. A reaction to form LiOH (or LiOD) was not identified; a possibility is the reaction $Li_2O + H_2$ (or D_2) → LiOH (or LiOD) + LiH (or LiD). Similar experiments using TPD, as well as IR, showed that hydride peaks were only observed after hydroxyl peaks were removed by heating to 400 °C while purging with an Ar + 0.1 mol% H_2 mixture. Kopasz et al. proposed that sites were available to form hydride after removal of hydroxyl.

Nishikawa et al. [32] showed that Li_2O can react with H_2 to produce H_2O. Li_2O particles were heated slowly to 700 °C in He to convert any LiOH (present as contaminant) to Li_2O; the sample temperature was then set to the experimental temperature (500–700 °C) while He/H_2 was passed through the Li_2O bed at 400 mL/min, and H_2 and H_2O concentrations were measured by gas chromatography and hygrometry respectively. The amount of H_2O produced was equal to the amount of H_2 consumed on a molar basis. It was also determined that the amount of H_2O generated was dependent on temperature rather than on amount of H_2 reactant. Further experiments using D_2 gas led Nishikawa et al. to conclude that H_2O and a nonstoichiometric lithium oxide were being formed, by the reaction $Li_2O + xH_2O \rightarrow Li_2O_{1-x} + xH_2O$. This reaction suggested by Nishikawa is not balanced; a balanced reaction would be $Li_2O + xH_2 \rightarrow Li_2O_{1-x} + xH_2O$. Also, reaction sequences from the additional experiments with D_2 that led to their preference for a nonstoichiometric reaction, were not given.

Stecura [3] showed that trilithium dioxide, Li_3O_2, forms from LiOH at elevated temperatures and lowered pressures, as follows: $6LiOH \rightarrow 2Li_3O_2 + 2H_2O + H_2$. The reaction was carried out at temperatures of 640–730 °C and pressures of $1.3–2.7 \times 10^{-3}$ Pa for 2880 min, with the reactant contained in metal alloy containers. Lattice parameters were determined for the compound by XRD; the structure was determined to be simple orthorhombic.

4. Studies of LiH hydrolysis reaction kinetics and reaction parameters

The same groupings used for the hydrolysis reaction products are used here to review studies on LiH hydrolysis reaction kinetics. However, an additional group 'very high H_2O concentrations,' is added to categorize reactions for which the products are Li^+ and OH^-. Kinetic rate expressions are presented when available, along with comparative rate data and mechanisms, and activation energies. The experiments are summarized in Tables 3 and 4.

The experimental parameters of surface area, pH, temperature, pressure, mixing, and impurities have all been observed as variables that can affect the reaction rates of LiH hydrolysis [39]. Therefore, separate sections are included in this review to discuss results that have been observed for several of these parameters. Specifically, sections discussing the effects of temperature and pressure, impurities, and both defects and surface area for LiH reactions with H_2O are presented.

4.1. Reaction kinetics for LiH at low H_2O concentrations

Machin and Tompkins [12] developed a kinetic expression, Eq. (1), for the production of H_2 from LiH hydrolysis based on their study of polycrystalline LiH particles in a vacuum reacted with

consecutive doses of high-purity H_2O vapor at 0–121 °C.

$$D = \frac{1}{t}\ln\left(\frac{a}{a-x}\right) - \frac{Cx}{t}, \quad (1)$$

$x = H_2$ pressure after time t; $a =$ final H_2 pressure; $t =$ time; C and D are constants in any particular run.

The expression incorporates parameters that vary with temperature and decrease as hydrolysis product accumulates. During their experiments, the researchers noted that the presence of hydrolysis products formed in varying quantities from previous exposure of H_2O vapor to LiH, had no effect on the rapidity and completeness of the removal of H_2O vapor from the gas phase. H_2O doses were removed from the gas phase within 1 min, but H_2 production continued for hours. They concluded that diffusion of sorbed H_2O to the reaction interface was not rate controlling. Activation energies calculated for the production of Li_2O_α and Li_2O_β. (where Li_2O_α reacts readily with H_2O and Li_2O_β does not react as easily with H_2O) were determined to be 2.5 kJ/mol and 32 kJ/mol, respectively.

Balooch et al. [16] studied hydrolysis of single crystal {100} LiD using a variety of techniques. The first technique combined Modulated Molecular Beam Mass Spectrometry (MMBMS) with Auger Electron Spectroscopy (AES). LiD was cleaved in a vacuum and then exposed to 1.3×10^{-5} Pa H_2O for ~4 min at RT. A plot of hydrogen production probability (fraction of times that a hydrogen producing reaction does occur out of the total number of possible reaction events) and surface oxygen coverage as a function of exposure to H_2O is shown in Fig. 8. Both H_2 and an oxygen-containing Li compound are the expected products of the hydrolysis reaction. A time lag in observing H_2, with respect to H_2O exposure, was observed (similar to Machin et al.); the lag increased as the hydrolysis product layer increased. In contrast to Machin and Tompkins, Balooch et al. suggested that the time lag of the H_2 was a result of the time required for an oxygen containing species to diffuse through the hydrolysis product and react at an interface. AES identified an 'oxygen containing species,' that was referred to as LiOH. However, no AES data were presented, and therefore the identity of the hydrolysis product was not clear. Because the H_2O concentrations were very low (at least 6 orders of magnitude lower than the other studies reviewed), the hydrolysis product may have been Li_2O.

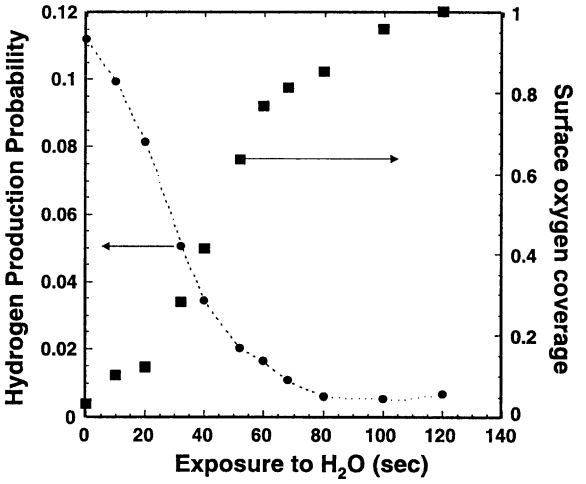

Fig. 8. H_2 evolution probability and surface O coverage as a function of single crystal LiD exposure time to 1.3×10^{-5} Pa H_2O in vacuum at RT using MMBSM [16].

Balooch et al. showed evidence that their pre-exposure LiD sample was not (fully) oxidized, which is unique among LiH hydrolysis experiments to date.

4.2. Reaction kinetics for LiH at high H_2O concentrations

Using SEM, Dinh et al. [20] studied single crystal {100} LiD exposed to air containing 1783 Pa H_2O at 27 °C. A corrosion layer is clearly evident in micrographs; after 1800 min, a layer ~18–20 μm thick developed, which is ~11 nm/min if a linear reaction rate is assumed. In a related SEM study, Balooch et al. [16] studied single crystal {100} LiD exposed to air containing 1584 Pa H_2O at RT for 3413 min. Fig. 9 is a graph of the thickness of

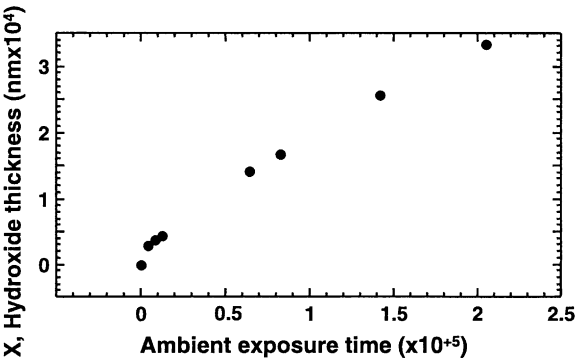

Fig. 9. LiOH layer thickness with time for single crystal LiD reacted with 1584 Pa H_2O in air at RT, as measured by SEM. The unit for the time is assumed to be seconds [16].

the hydrolysis product vs. time. The graph shows an initial rise, followed by a linear growth rate of ~8 nm/min. The rates take into account the geometrical constraints to growth that occurred at corners of a rectangularly shaped sample. The hydrolysis product film was described as $LiOH \cdot H_2O$, which appears to be presumed from the H_2O level of exposure. The authors suggested that movement of an oxidant through the relatively thick $LiOH \cdot H_2O$ layer would occur by diffusion through microcracks.

Balooch et al. also used atomic force microscopy to measure the growth rate of hydrolysis products by calculating changes in electric potential through a hydrolysis film over time. They exposed a sample of single crystal LiD to 1584 Pa H_2O in air for up to ~1400 min at (we assume) RT and monitored the thickness of the hydrolysis layer. The growth rate of $LiOH \cdot H_2O$ was 0.363 nm/min and was linear with time, as shown in Fig. 10; the growth rate of LiOH was 21.8 nm/min and was also linear.

Powell et al. completed an IR study [28] to determine the kinetics of LiH hydrolysis. In this work, a polycrystalline LiH pellet exposed to a specific H_2O concentration in an Ar-filled glovebox, where the H_2O concentration would have been relatively constant. The sample was exposed to 7 Pa H_2O (assuming ambient pressure – close to typical LiH glovebox very slightly positive pressure – and that the literature value of 73 ppm is in units of volume) at RT (we assume) for 30 000 min. Diffuse reflectance FTIR was used to quantify the amount of hydrolysis product formed; samples were also weighed. Fig. 11 shows the quantity of LiOH formed as a function of time. The weight gain vs. time curve matched the analogous FTIR curve; both showed first parabolic and then linear behavior. The growth rate of LiOH, calculated from the linear portion of the curve, is ~82 mmol/min.

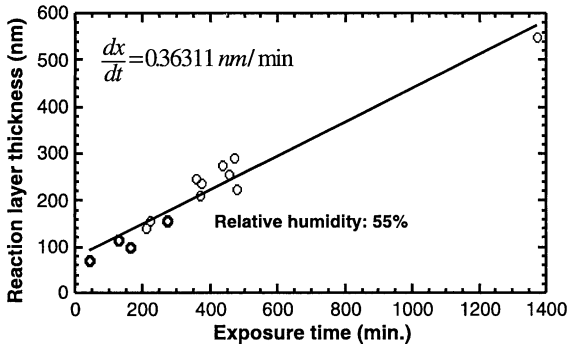

Fig. 10. $LiOH \cdot H_2O$ layer thickness as a function of single crystal LiD exposure time to 1584 Pa H_2O in air, as measured by AFM [16].

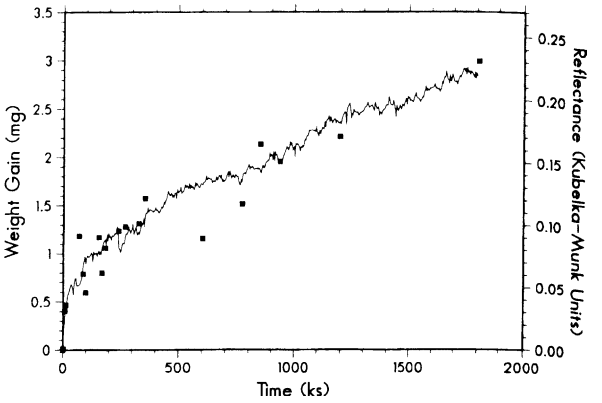

Fig. 11. Weight gain and IR data for LiH exposed to 7 Pa of H_2O (estimated value) in Ar for ~30 000 min (500 h). The continuous curve shows weight gain while squares show LiOH quantity from IR measurements [28].

Holcombe [40] determined a hydrolysis reaction rate from weight gain measurements for polycrystalline LiH pellets alternately exposed to air containing 317 Pa H_2O and dry Ar at (we assume) RT. This exposure lasted a total of 42 000 min. The weight gain was found to be linear with time after a 1 μm film of LiOH had grown on the LiH surface. The equation was as follows:

$$W = 14.2 + 0.549t \quad (2)$$

W = weight gain, mg/cm$^2 \times 10^2$; t = time, h.

Broughton [15] also studied LiH hydrolysis kinetics from weight gain measurements. LiH polycrystalline particles were exposed to 500 mL/min flowing Ar containing 0.55 kPa or 1.9 kPa of H_2O at 20–25 °C for up to several thousand minutes and weighed periodically. Gravimetric measurements were also completed for LiH polycrystalline pellets exposed to 1000 mL/min flowing Ar containing 0.63, 1.5 or 2.6 kPa of H_2O at 37–41 °C. Experiment pressures were not reported, but were likely to be slightly positive (<1000 Pa), as the measurements were completed in a glovebag or glovebox. Results are shown in Figs. 12 and 13. For both sets of experiments, the weight increase shows an initial rise and subsequent linear increase with time. Increased H_2O levels increased the rate of reaction. A simple slope calculation in the linear regime of weight gain yields the following reaction rates: 0.50 mg/min for 0.55 kPa H_2O, and 1.2 mg/min for 1.9 kPa of H_2O, both flowing at 500 mL/min, 0.42 mg/min for 0.63 kPa H_2O, 0.53 mg/min for 1.5 kPa H_2O,

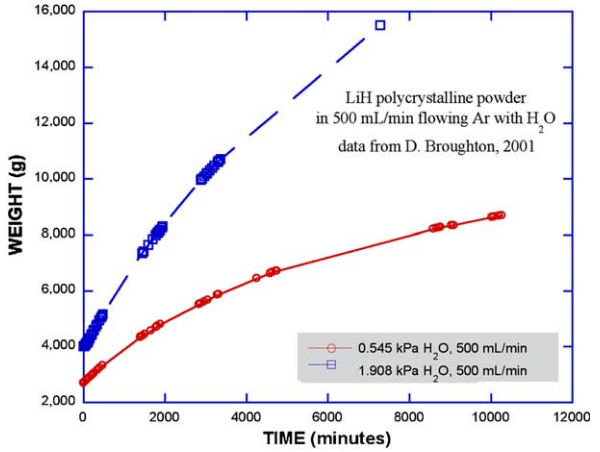

Fig. 12. Increase in weight with time for polycrystalline LiH particles exposed to 0.55 kPa or 1.9 kPa H_2O in 500 mL/min flowing Ar at 20–25 °C [15].

and 0.71 mg/min for 2.6 kPa H_2O all flowing at 1000 mL/min. In the first set of experiments, Broughton calculated reaction orders that were close to first order with respect to H_2O, specifically 1.11 for the reaction at 0.55 kPa H_2O and 1.06 for the reaction at 1.9 kPa H_2O, both flowing at 500 ml/min. For the second set of experiments, Broughton calculated polynomial fits for data collected between ~120 and 960 min as seen below. Analysis of rate orders showed that the reactions were first order during the latter portion (after several hours) of the reactions.

$$R = 0.8560t^3 + 1.338t^2 - 0.7325t + 0.2002 \quad \text{for 0.63 kPa } H_2O, \text{ flowing at 500 mL/min} \tag{3}$$

$$R = 0.6810t^3 + 1.159t^2 - 0.6825t + 0.2093 \quad \text{for 1.5 kPa } H_2O, \text{ flowing at 500 mL/min} \tag{4}$$

$$R = 0.5947t^3 + 0.9395t^2 - 0.5448t + 0.2059 \quad \text{for 2.6 kPa } H_2O, \text{ flowing at 500 mL/min} \tag{5}$$

R = weight gain rate, % mass increase/day; t = time (h).

Broughton also investigated the use of solid state nuclear magnetic resonance spectroscopy for characterizing LiH hydrolysis, but found that the technique did not quantitate well due to long nuclear spin relaxation times in LiH.

Several studies have been completed to determine the viability of LiH hydrolysis as a hydrogen fuel source, specifically for underwater vehicles or fuel cells; these studies include work by DeVries [41], Pitcher et al. [42], and Kong et al. [43,44]. Because H_2 is the product of interest, hydrolysis reactions were quantified by measurements of H_2 evolution. Water levels in these H_2-fuel experiments are often sufficient to produce Li^+ and OH^- in aqueous solution; however, the kinetic expressions were developed by monitoring H_2 product levels and, therefore, should apply to the production of LiOH (along with H_2).

In an early study of this type, DeVries [41] mixed polycrystalline LiH particles of differing sizes in a finite quantity of H_2O of various purities and concentrations, at 21 °C and varying environmental pressures, by intimately mixing the materials for 6 min. The gaseous environment was not specified, except in cases where N_2 pressurization was used. He determined that use of H_2O at 25 times the H_2O/H_2 stoichiometric excess ratio resulted in a complete reaction and a greater reaction rate than was obtained when smaller quantities of H_2O were used. Use of H_2O levels greater than 25 times the H_2O/H_2 stoichiometric excess ratio did not increase the reaction rate. H_2 production vs. time curves (Fig. 14) show a rapid increase, followed by a transition to a zero slope region or to a linearly increasing region. The shape of the curve depended on various experimental parameters such as pressure, purity levels, and surface areas, which are discussed in a later section.

Pitcher et al. [42] continued H_2 fuel studies using an experimental setup consisting of a gas pump, a reaction chamber, and a gas collection chamber. LiH polycrystalline pellets of varying sample surface areas were exposed to liquid H_2O of varying purities at rates ranging from 1 to 11.2 mL/min for typically 30–90 min. The reaction chamber was pressurized to varying levels using Ar (in addition to H_2O). The temperature of the LiH reaction was 90 °C. Fig. 15 shows a typical curve for H_2 evolution with time. The curve shows an initial rise and then becomes linear with time, having a final slope of essentially zero where the reaction does not proceed further. Reaction rates were calculated from the linear portion of the H_2 generation curves, range from 3 to 15 mmol/min H_2, and are listed in Table 3. The rates increased with increasing H_2O flow rate. Of the variables studied, the reaction rate was most heavily influenced by the H_2O flow rate.

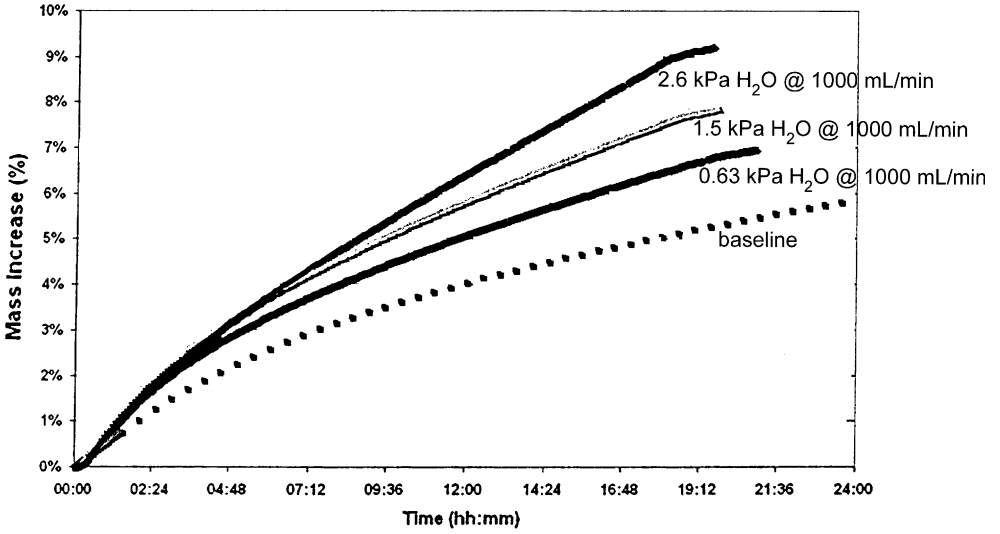

Fig. 13. Increase in weight with time for polycrystalline LiH pellets exposed to 0.63, 1.5, or 2.6 kPa H_2O in 1000 mL/min flowing Ar at 37–41 °C [15]. The present authors added H_2O concentrations in Pa units. Baseline LiH was exposed to Ar with no intentionally added H_2O.

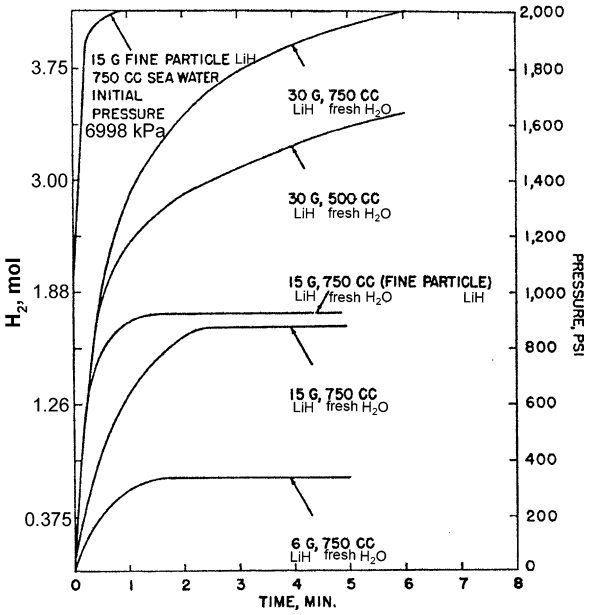

Fig. 14. H_2 pressure vs. time for LiH polycrystalline particle hydrolysis at 21 °C and at (assumed) 101.3 kPa (except for one measurement at 6998 kPa) [41]. The present authors added the units for H_2 production in mol.

Effects of pressure, impurity contents, and surface area discussed in a later section.

The most recent study of the H_2 fuel genre was published by Kong et al. in a two-part paper [43,44]. In Part I, several metal hydrides were studied for their potential as H_2 fuel sources. CaH_2 and LiH were considered the most promising materials and, thus, were studied the most extensively. In the first paper, LiH polycrystalline particles were either exposed to drops of deionized liquid H_2O or placed in a deionized H_2O vapor environment. H_2O vapor was shown to be more effective in producing H_2 gas than H_2O liquid. The experiments were all completed at 25 °C, although it was noted that temperatures increased during the experiments from the considerable heat produced by the hydrolysis reactions. The experiment environmental pressures were ~101.3 kPa (ambient pressure); the sample environments were not noted but were likely air. The hydrolysis reactions proceeded to 90+% completion. Curves for H_2 production as a function of exposure time showed an initial rise followed by linear behavior and finally a zero slope when the reaction completed (Figs. 15 and 16). The linear reaction rate for H_2 production (in moles) from LiH (in g) was 2.8×10^{-5} mol/g s for 0.05 mL drops of H_2O on LiH particles.

In Part II of the paper by Kong et al. [44], LiH polycrystalline particles were placed in a container with a H_2O/KOH solution at 22 °C. LiH samples were not in direct contact with liquid H_2O, but were held above the solution and reacted with the H_2O vapor. The H_2O vapor pressure was controlled by the KOH addition to the H_2O; H_2O was always present in a H_2O/H_2 stoichiometric excess, i.e. more H_2O was available than H_2 that could be produced for the amount of LiH. Sample environments and pressures were not specified, and, thus, were likely air at ambient pressure (101.3 kPa). Increasing

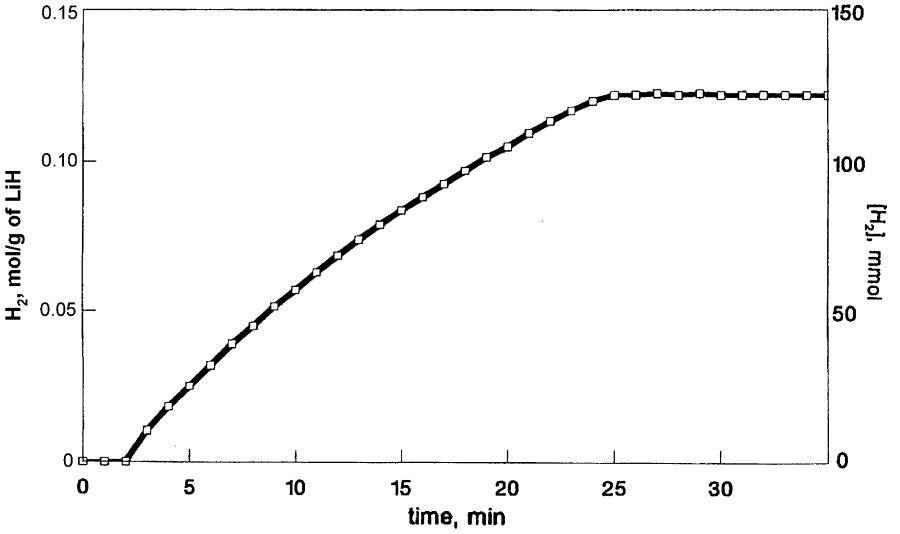

Fig. 15. H_2 evolution with time for hydrolysis of LiH polycrystalline pellets reacted with H_2O flowing at 0.11 mL/min in Ar, at a pressure of 1×10^6 Pa. The reaction rate for the curve (between 4 and 24 min) was determined to be 5.06 mmol/min H_2 produced [42]. The present authors added the units of H_2 production in mol/g of LiH.

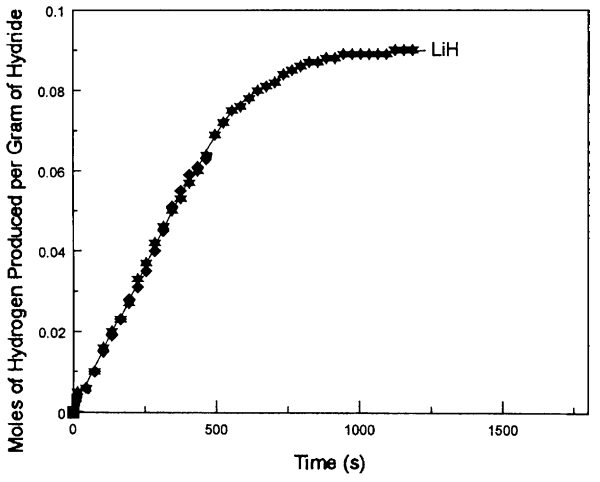

Fig. 16. H_2 evolution with time for 0.05 mL of liquid H_2O dropped onto polycrystalline LiH particles every 15 s [43].

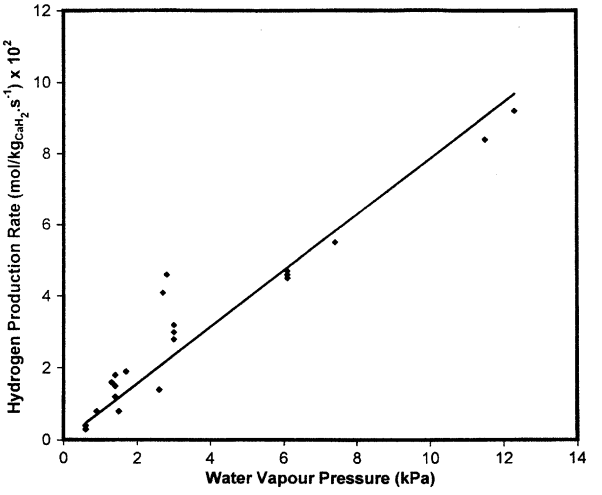

Fig. 17. Effect of H_2O concentration on the H_2 production rate production rate for CaH_2 hydrolysis [44].

H_2O vapor concentration (reacted with CaH_2) linearly increased the reaction rate to produce H_2, as shown in Fig. 17 (results for LiH are expected to be similar). Curves of the H_2 generated vs. time show an initial rise followed by a linear slope, as seen in Fig. 18. A model was developed for the hydrolysis reaction rate (Eq. (6)) by using a diffusion-limited rate determining step and by estimating boundary layer thicknesses and effective H_2O diffusivities. Curves resulting from the model equation, using the parameters of the LiH hydrolysis experiments, are shown in Fig. 18.

$$f_s = 1 - \sum_{n=1}^{\infty} \frac{4L^2 \exp(-\beta_n^2 Dt/r_b^2)}{\beta_n^2(\beta_n^2 + L^2)}, \tag{6}$$

f_s = fractional conversion of a hydride slab; D = diffusivity of H_2O through; r_b = radius of the hydride bed; β = constant; t = time; $L = r_b\alpha/D$; α = average penetration rate of the water vapor.

Linear kinetics were almost invariably observed by researchers for LiH hydrolysis reactions with 'high' H_2O concentrations supplied at steady state. Under these conditions, linear kinetics may result from diffusion through a thin layer of constant

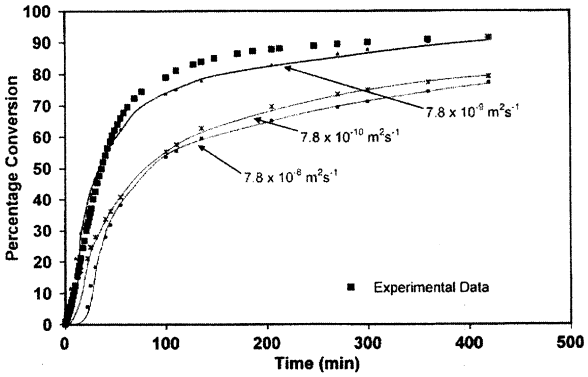

Fig. 18. Model and experimental data for H_2 evolution with time for LiH polycrystalline particles reacted with deionized H_2O vapor at 22 °C. The model curves show the effect of varying H_2O diffusivities [44].

thickness. A thin layer is consistent with a hydrolysis product structure that comprises Li_2O between LiH and LiOH layers. Upon reaching an equilibrium thickness for specified conditions, this Li_2O remains a constant thickness, but moves deeper into the sample as the LiOH grows. Oxygen must diffuse across this Li_2O layer, and is the rate controlling process. This results in overall linear kinetics for large area LiH. Particulate LiH may differ in reaction order.

4.3. Reaction kinetics for LiH at very high H_2O concentrations

Leckey et al. [45] studied LiH hydrolysis with very large quantities of H_2O in an effort to better quantify the hazard potentials of reactions. Leckey and Nulf submerged a 0.80 cm radius × 1.80 cm thickness pellet of polycrystalline LiH in 1800 mL of H_2O that was surrounded by a cooling bath to keep the temperature constant at 34–36 °C. The change in conductivity induced by the Li^+ and OH^- formed from dissolved LiOH was measured as a function of reaction time. The reactions ($LiH + H_2O \rightarrow LiOH + H_2$ and $LiOH \rightarrow Li^+ + OH^-$) slow as the H_2O becomes saturated with dissolved LiOH. Fig. 19 shows concentration of dissolved LiOH as a function of reaction time along with a least squares fit. The data show a third order dependence of concentration on time. Leckey and Nulf developed a 'nonequilibrium thermodynamic-based model' to describe the reaction rate behavior, which is given below (Eq. (7)). The rate is described as proportional to the surface area of the LiH multiplied by the difference in chemical activity of the reaction product, LiOH, between the solid phase and the aqueous phase. The model was used to predict H_2 generation rates for LiH in dilute or moderately saturated H_2O. The model predicted only a small dependence of reaction rate on temperature. An activation energy for LiH hydrolysis was experimentally determined to be −13 kJ/mol. Leckey and Nulf did not understand the negative activation energy, but they did suggest it may be an effect of an H_2 gas layer formed at the solid/solution interface.

$$\frac{dc}{dt} = \alpha k A(t)\left(1 - \frac{\gamma_{\pm}(c)t}{\gamma_{\pm,s}} \times \frac{c}{c_s}\right), \tag{7}$$

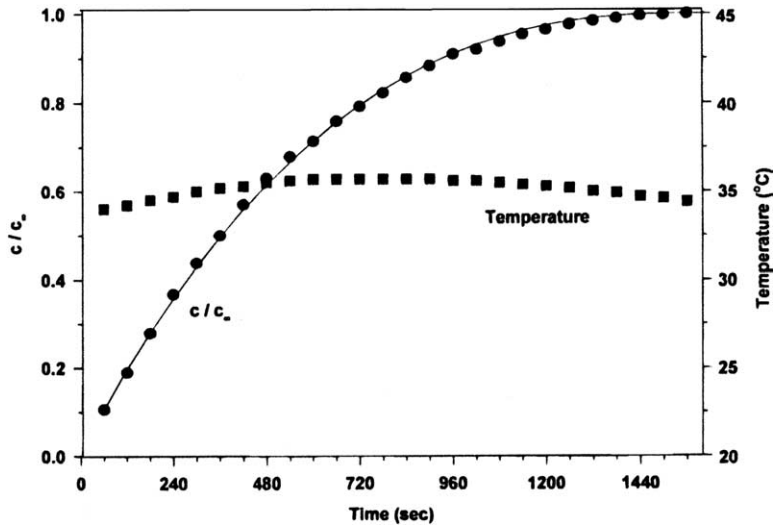

Fig. 19. Extent of reaction and solution temperature as a function of reaction time for a LiH polycrystalline pellet in liquid H_2O [45].

$\alpha = \rho/M_w V$; ρ = mass density of solid LiH; M_w = molecular weight of LiH; V = volume of LiH; c = concentration; t = time; k = rate constant for LiH reacted in terms of depth per time; $A(t)$ = surface area of LiH as a function of time; $\gamma_{\pm}(c)$ = activity coefficient of LiOH in solution at any time (concentration dependent); $\gamma_{\pm,s}$ = activity coefficient of LiOH in saturated aqueous solution.

Rozenband completed a study in which a LiH pellet was immersed into a container of H_2O beneath an air atmosphere [46]. The temperature of the LiH pellet was monitored to determine the rate of heat generation produced. The resultant temperature vs. time curve is shown in Fig. 20. The time scale is very small, <1 s. Rozenband interpreted the curves to have an initial linear growth region, followed by a diffusion limited region, where the reaction rate was determined by diffusion of an oxidant to the reaction interface. This latter portion of the curve gives a heat production rate of ~2.5 °C/s for LiH reaction in H_2O. Rozenband determined that the initial growth region was first order and developed an expression for heat generation shown in Eq. (8) where $Qk_0 = 1.4 \times 10^{19}$ J m/mol s.

$$q = Qk_0C_0 \exp\left(-\frac{6210}{RT}\right), \tag{8}$$

q = heat of reaction, J; Q = heat of reaction, J/mol; k_0 = pre-exponential factor, m/s = 3.4×1020 where; C_0 = volumetric concentration of oxidant; R = gas constant, J/(mol K); T = temperature, K.

Additional experiments were completed using H_2O containing additions of 10%, 20%, and 30% (no unit was specified) ethanol. Ethanol was used to lower the available H_2O concentration; Rozenband indicated that LiH reacts very little with ethanol (although Messer [18] has documented strong reactions with other alcohols). The increasing amounts of ethanol slowed the temperature increase of the aqueous solution, implying that the LiH hydrolysis reaction rate had decreased. Data are also shown in Fig. 20.

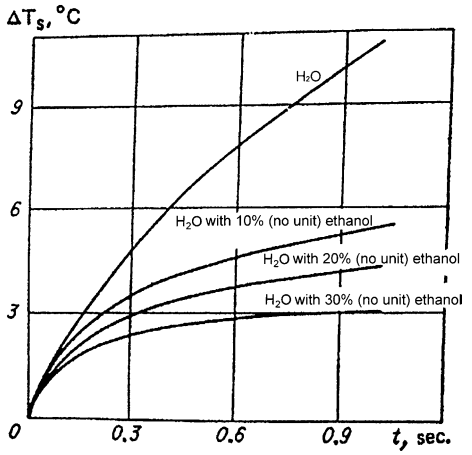

Fig. 20. Change in temperature as a function of time for polycrystalline LiH pellets immersed in a container of liquid H_2O in air [46].

4.4. Temperature and pressure effects on LiH–H_2O reaction kinetics

LiH hydrolysis involves two reactants in the studies reviewed here, LiH (solid) and H_2O (gas or liquid in the reviewed studies), either or both of which could be at different temperatures at the start of or during reactions. This fact introduces a potential for variation between experiments. One can imagine three scenarios. In the first, the H_2O and sample are both at the same temperature; for example, when LiH and H_2O are both at RT. In the second scenario, the H_2O is heated but the LiH is not heated; an example of this would be heated, flowing, H_2O gas passing over an LiH sample. In the final type of experiment, the H_2O is not heated but the LiH is heated; for example LiH sitting on a hotplate in air. In the cases where the LiH and H_2O are at different temperatures, the local environment near to the solid LiH may be different than expected, unless the two materials have equilibrated to the same temperature (such as might occur for heated, flowing gas passing over a LiH sample). Unfortunately, specific information on reactant heating is not always available.

A further complication in reporting reaction temperatures is that many of the LiH hydrolysis reactions are quite exothermic i.e., they create considerable heat. As an example, an experiment by Kong et al. [43] in which LiH particles were reacted with H_2O vapor at a nominal 22 °C, showed that the interior of the LiH bed reached 45 °C. A sample temperature may therefore be greater than (or less for an endothermic reaction) an experimenter's stated value. In a few cases, experimental temperatures were monitored to obtain the 'true' value; in most cases, however, either the environmental temperature was not reported or the monitoring process was not made clear. While an error in temperature measurement may not readily seem to be a concern for trend analysis, the Li–O–H system has been reported to have a phase transition at ~50 °C at

ambient pressures, which could affect results [16]. This is in the range of temperatures that could be generated from hydrolysis at RT. Other phase transitions may be present at the temperature ranges and pressures of experiments, and therefore, temperature results should be considered carefully.

Using MMBMS, Balooch et al. [16] studied temperature effects on LiD hydrolysis using single crystal LiD in ultra-high vacuum exposed to H_2O pressures of 1.3×10^{-5} Pa. The heating method was not discussed, but a schematic of the experimental setup shows that the LiH was heated. The researchers found little effect of temperature on H_2 production probability (resulting from LiD hydrolysis) in the range of ~RT to 230 °C. The results are shown in Fig. 21. As discussed previously, the hydrolysis product at such low H_2O levels may have been Li_2O. Balooch et al. suggests that the insensitivity to temperature indicates a negligible activation barrier to hydrolysis of 'pure' i.e. unoxidized LiD.

Dinh et al. [27] completed a further experiment to determine temperature effects by measuring the thickness of hydrolysis products using SEM for LiD exposed for 1800 min to moist air at either 27 °C or 66 °C. The heating conditions for this experiment were undefined, however, it is clear that the LiH was sitting in air at 50% relative humidity. Therefore, in the experiment at 66 °C, the temperature should apply to the solid LiH, but not necessarily to the H_2O. If one assumes that the H_2O was 27 °C (as in the companion experiment), then the H_2O concentration is 1783 Pa. If the H_2O was at a higher temperature, then the H_2O concentration would be greater. The product layer in the RT sample was 4–7 times thicker than in the higher temperature sample. The researchers suggested that $LiOH \cdot H_2O$ is present in the samples treated at higher temperatures, as a phase transition occurs at ~50 °C between LiOH and $LiOH \cdot H_2O$. The $LiOH \cdot H_2O$ phase was suggested to have a lower sticking probability and a increased desorption rate for H_2O molecules (as compared with LiOH), and therefore the reaction rate should decrease with increased temperature.

Balooch et al. [16] also completed gravimetric studies at various temperatures. They exposed LiD single crystal to 100% relative humidity (2338 Pa H_2O assuming H_2O is always at initial 20 °C and at ambient pressure) in N_2 (pressure not given), and measured the weight gain. The details of heating were not given, but if we assume a typical thermogravimetric setup, then the LiH was heated and the H_2O was not. The weight gains were linear with time at all temperatures studied. At RT, the weight gain rate was reported as 7.6 O atoms/s. The rate of weight gain showed a strong decrease with temperature between ~20 and 50 °C and a small decrease with temperature between ~50 and 175 °C, as shown in Fig. 22. The authors suggested that the temperature dependence might indicate a diffusion-controlled process. The hydrolysis products were not identified, but the primary product was likely $LiOH \cdot H_2O$.

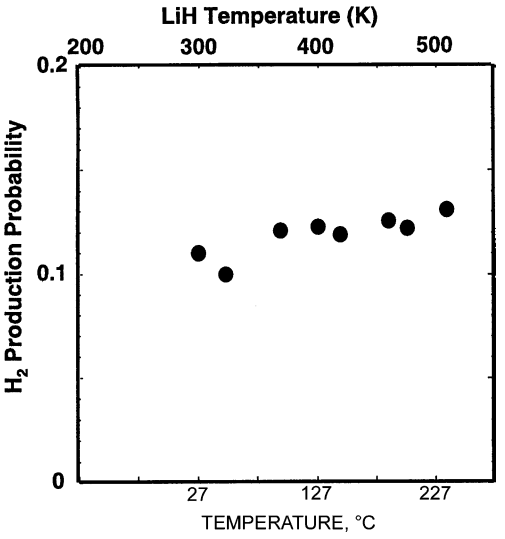

Fig. 21. Hydrogen probability determined by MMBSM as a function of temperature for LiD single crystal exposed to 1.3×10^{-5} Pa H_2O in vacuum [16]. The present authors added the units of temperature in Celsius.

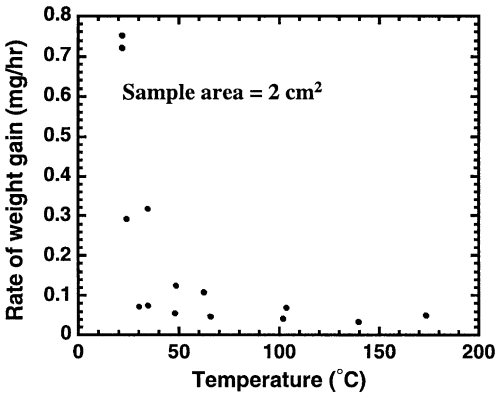

Fig. 22. Weight gain rate as a function of temperature for LiD single crystal exposed to 2338 Pa H_2O in N_2 [16].

Broughton completed his gravimetric studies for polycrystalline LiH pellets in Ar with H_2O at glovebox pressures and several temperatures, namely, 33 °C, 39 °C, and 57 °C; the temperatures reflect the temperature of the H_2O gas. The measured H_2O levels of the experiment were 1.3 kPa (13 000 ppmv) H_2O at 33 °C, 0.93 kPa (9200 ppmv) H_2O at 39 °C, and 1.3 kPa (13 000 ppmv) H_2O at 57 °C, all flowing at 1000 mL/min. The H_2O levels were intended to be equivalent by volume, but the measured H_2O levels showed that the reaction at 39 °C was at a somewhat lower H_2O level. Measurements lasted 7200 min. The data are shown in Fig. 23. During the initial 480–600 min, the greatest weight gain, i.e. reaction rate, was observed at the intermediate temperature (39 °C) followed by the rate at the highest temperature and then at the lowest temperature. This result is particularly intriguing as the 39 °C reaction was at a lower H_2O level and would therefore have been expected to show a slower reaction. In the last stage of the experiment (~5700–6600 min), the lowest temperature reaction showed the greatest reaction rate. In a further set of experiments, polycrystalline LiH pellets were exposed to 0.95 kPa H_2O (one set) or 1.3 kPa H_2O (another set) in Ar at either 33 or 39 °C. The difference in reaction rates was small, however, the lower temperature measurements showed greater reaction rates (Fig. 24). Broughton suggested that different products may form at the different temperatures (similar to Balooch et al.), which may have led to the mixed effects of temperature.

Cecala et al. [47] measured the reaction rate of polycrystalline pellets of LiH mixed in very large quantities of liquid H_2O at various temperatures from RT to ~100 °C. The rates were determined from measurements of the time of bubble formation (i.e., H_2 gas) and of change in solution conductivity as a LiH pellet (0.32 inner radius × 1.67 cm outer radius × 1.52 cm height) was submerged in ~4.5 L H_2O. Fig. 25 shows a plot of the extent of reaction vs. reaction time at 23 °C and 95 °C. The reaction for the experiment at 23 °C completed in ~4 min while the 95 °C reaction was much slower, completing at ~10 min. Cecala et al. suggested that the cause for the decline in reaction rate with increasing temperature was a slowed dissolution of LiOH at increased temperatures. The reaction rate was modeled by the Arrhenius equation given in Eq. (9) (and by a power function). Values for k were determined to be 1.53×10^{-3} to 3.05×10^{-3} cm/s, while A was 1.72×10^{-4} cm/s and E was −6.7 kJ/mol. The activation energy was negative, similar to results by Leckey et al. [45].

$$k = Ae\frac{-E}{RT}, \tag{9}$$

k = rate constant, cm/s; A = pre-exponential factor, cm/s; E = activation energy, kJ/mol; R = gas constant, kJ/mol K; T = temperature, K.

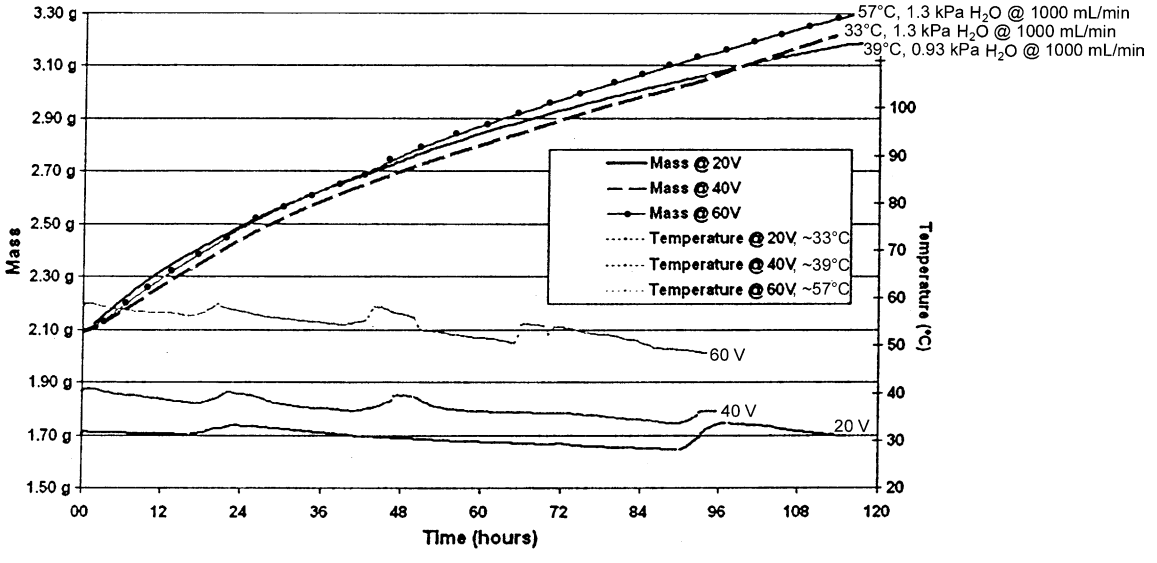

Fig. 23. Weight gain rate as a function of temperature for polycrystalline LiH pellets exposed to flowing H_2O in Ar [15]. The present authors added the curve labels.

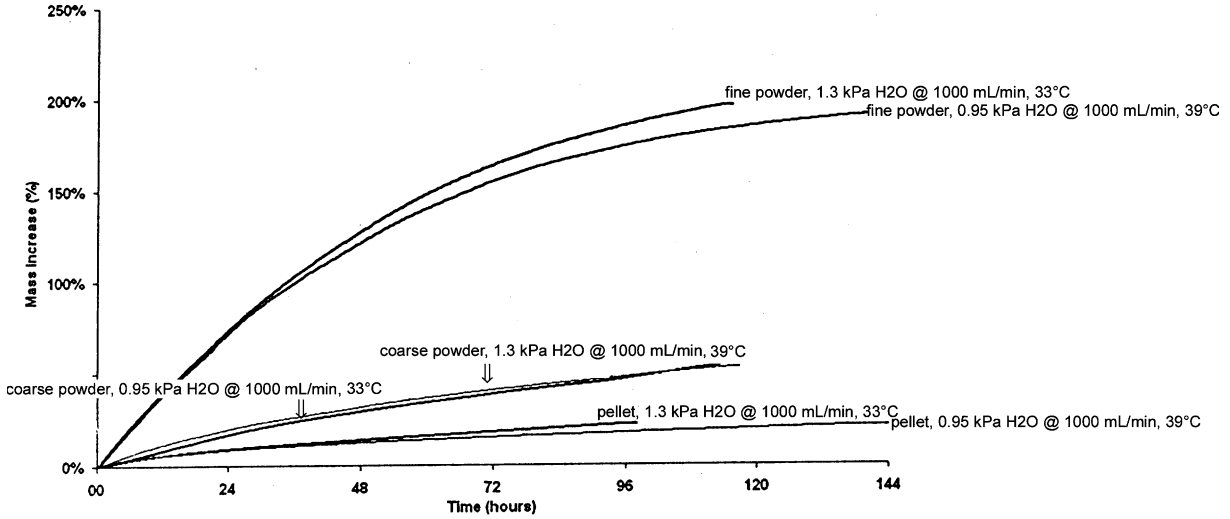

Fig. 24. Weight gain rate as a function of time for LiH samples with various surface areas exposed to flowing H_2O in Ar [15]. The present authors added curve labels.

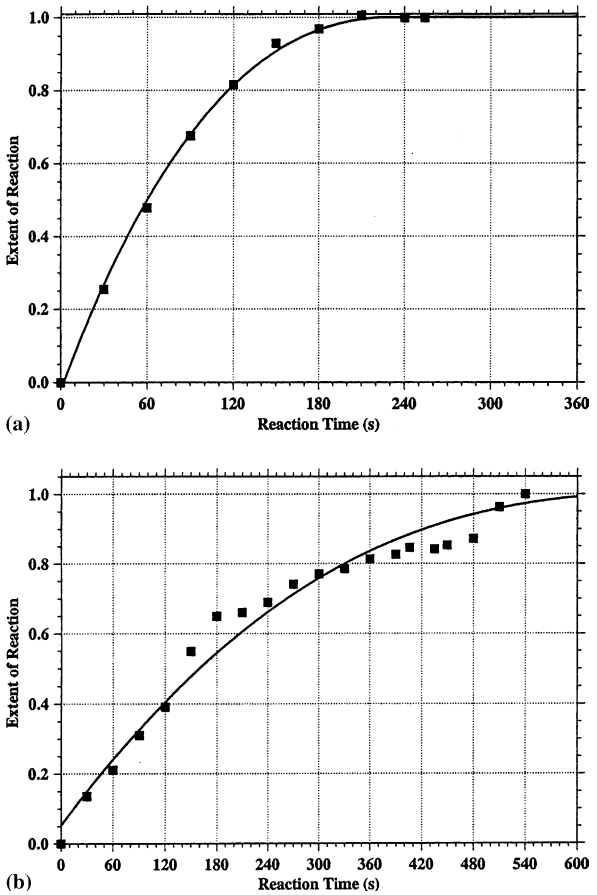

Fig. 25. Extent of reaction as a function of reaction time for polycrystalline LiH pellets immersed in a container of H_2O that was open to air at (a) 23 °C and (b) 95 °C [47].

Kong et al. [44] obtained results opposite to those of Balooch et al. [16] and Cecala et al. [47]. In studies discussed earlier, H_2 production was monitored while LiH particles were exposed to deionized H_2O vapor in a container of air at temperatures in the range of 0–60 °C. Temperatures were recorded at multiple locations, but the location of the reported values was not specified, therefore it is unclear whether the reported temperature reflects the temperature of the LiH or the H_2O. Increased temperature was found to give a small linear increase in H_2 production rates (Fig. 26).

DeVries [41] studied the effect of environmental pressures on H_2 production during LiH hydrolysis. By mixing LiH polycrystalline particles in liquid

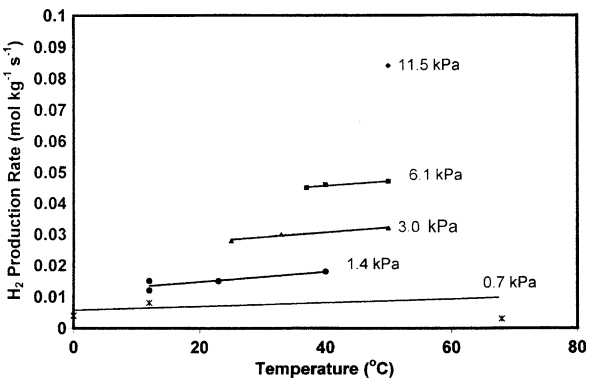

Fig. 26. H_2 evolution as a function of temperature for LiH polycrystalline particles exposed to various H_2O vapor pressures (noted on plot) in air [44].

H_2O while pressurizing the container with N_2, DeVries [41] found that increased pressure greatly increased reaction rates. Data are shown in Fig. 14, in which curves at 101.3 kPa (ambient) and 6895 kPa are compared. The high-pressure curve shows a very rapid initial rate of H_2 production. DeVries suggested that the increase in reaction rate with pressure could be explained by a suppression of surface-passivation that results from absorbed hydrogen at the $LiH \cdot H_2O$ interface. Leckey et al. [45] also mentioned this phenomena, as a possible explanation for the negative activation energy that he calculated for LiH hydrolysis.

Pitcher et al. [42] showed a different effect of pressure. In experiments in which LiH pellets were reacted with liquid distilled H_2O, increased pressure (using Ar) led to a small decrease in reaction rate for pressures ranging from 250 kPa to 1500 kPa. The authors did not provide an explanation for the suppression of the reaction rate with increasing pressure.

The bulk of the results regarding the effects of temperature and pressure on the reaction rate of LiH hydrolysis showed that the reaction rate decreased with increasing temperature; however, not all the results agreed and some were directly opposed. Much less data are available showing the effects of pressure; two studies showed different results. The 'first glance' reason for the disparities might be that experimental conditions are different; indeed as discussed earlier, the need for accurate and specific information on temperature measurements is needed for proper interpretation, but is frequently missing. It may also be true that the effects of various temperatures and pressures cannot be globally applied in a simple manner to all hydrolysis experiments, e.g., the effect of temperature in a low H_2O regime might not be the same as the effect in a high H_2O regime.

Temperature and pressure effects may potentially be explained in terms of diffusion of an oxidizing species across hydrolysis layers. As thickness of a product layer changes with temperature or pressure, the diffusion length changes, and therefore, the time to diffuse. Hydrolysis layers with very open structures, on either a crystalline or microstructural level, may not limit diffusion, but a more densely packed structure could create diffusion limits. In the unusual and extreme case of no oxidation layer (as suggested for Balooch et al. [16]), there would be no effect of temperature changes during hydrolysis. Because LiH hydrolysis produces multiple product layers, the final dependence on temperature or pressure would be a combination of diffusion effects from the different layers. Kong et al. [44] developed their LiH hydrolysis rate model with a dependency on H_2O diffusivity.

Specifically, for a $LiOH/Li_2O/LiH$ hydrolysis layer structure, the thickness of the Li_2O layer is controlled by the activities of oxygen and hydrogen on either side of the layer. We believe that the observed linear reaction rates are therefore the product of diffusion across a moving layer of (effectively) constant thickness. As temperature increases, the thickness of the Li_2O layer is expected to increase [22,23], which would result in a net decrease in the overall reaction rate.

4.5. Impurity effects on $LiH–H_2O$ reaction kinetics

Holcombe [40] investigated the use of lithium compound barrier layers, specifically a C-containing compound and an F-containing compound, to reduce the reaction rate between LiH and H_2O. In the first case, pellets of polycrystalline LiH were pre-exposed to 317 Pa H_2O for 16 h (exposure to H_2O was previously found necessary for CO_2 to react with LiH to form Li_2CO_3), and then to CO_2 (or Ar for control samples) for 3960 min before a final exposure to 317 Pa H_2O for 42 000 min. Samples pre-exposed to CO_2 showed a 50% decrease in weight gain over a 1440 min period as compared with control samples, and a 19% decrease over 42 000 min. The weight gain was linear with time, as shown in Fig. 27 and as described by Eq. (10) given below. The microstructural appearance of CO_2 treated samples did not change as compared with analogous non-CO_2 treated samples. The phase of the C-containing layer was not identified by the researchers, however, it can reasonably be expected to contain Li_2CO_3 from reports in other literature [28]. While a barrier layer is not strictly an impurity in a hydrolysis reaction, the effect of Li_2CO_3 (which is thermodynamically favorable to form between LiOH and CO_2 – a typical component of H_2O) is demonstrated in this experiment.

$$W = 14.0 + 0.446t, \tag{10}$$

$W =$ weight gain, $mg/cm^2 \times 10^2$; $t =$ time, h.

Broughton [15] showed that a $LiOH–CO_2$ reaction is thermodynamically predicted to have a ten-fold increase in rate over a $LiH–H_2O$ reaction. Thus, the presence of CO_2 may dramatically interfere with LiH hydrolysis.

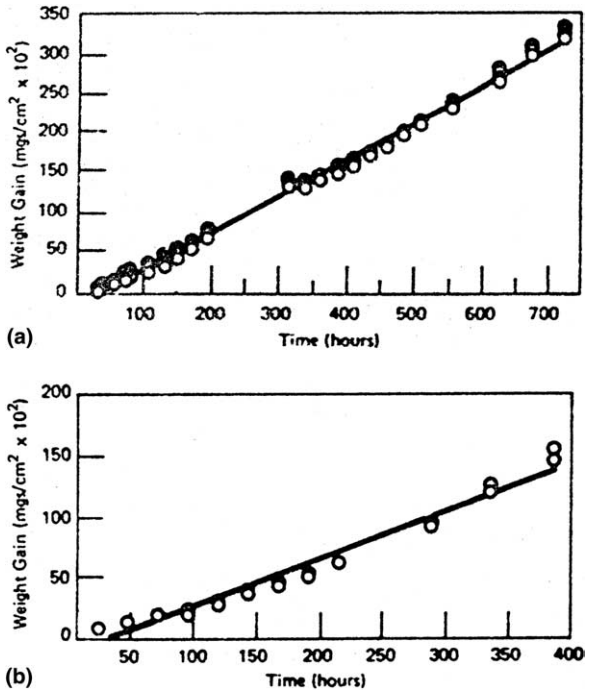

Fig. 27. Weight gain as a function of H_2O exposure time for LiH polycrystalline pellets pre-exposed to (a) CO_2 and (b) F [40]. The reference does not give a meaning for open data points as compared to solid data points.

H_2O may also contain fluorine as an additive. In the experiment testing the effect of a F-containing barrier layer, samples were treated in the same way as described above, but using fluorine as the pre-exposure gas. The fluorine treated samples showed a 31% decrease over a 385 h period in weight gain as compared with control samples (Fig. 27). The reaction rate for fluorine treated samples was described as linear with time, as given in Eq. (11). The phase of the F-containing layer was not identified, but one could expect the fluorine atom to substitute the hydrogen atom to form LiF.

$$W = 18.2 + 0.386t, \tag{11}$$

$W =$ weight gain, $(\mathrm{mg/cm^2}) \times 10^2$; $t =$ time, h.

The study by DeVries [41] (described earlier) included the use of seawater as a reactant as well as controlled additions of various liquids, typically oils that would not react with LiH, to H_2O. The composition of 'seawater' was not provided by DeVries, however, we provide a recipe for artificial seawater that reflects ASTM D1141-98 [48] in Table 5. The effect of seawater could not be singled out from other changing parameters in the experiments. It was noted, however, that insoluble precipitates formed upon completion of the reactions, which did not affect equilibrium or reaction rates considerably. Other additives, such as DC200 or hydraulic oil, did slow the reaction rate, although paint thinner apparently had no rate effect.

Table 5
Chemical composition of artificial ocean water [48]

Compound	Concentration, g/L
NaCl	24.53
$MgCl_2$	5.20
Na_2SO_4	4.09
$CaCl_2$	1.16
KCl	0.695
$NaHCO_3$	0.201
KBr	0.101
H_3BO_3	0.0207
$SrCl_2$	0.025
NaF	0.003

The study by Pitcher et al. [42] also included the use of liquid seawater as a reactant as well as liquid distilled H_2O for hydrolysis reactions with LiH polycrystalline pellets. The seawater gave an ~11% lower rate of H_2 evolution as compared with distilled H_2O. Pitcher et al. indicated that the solubility of $LiOH \cdot H_2O$ is lower in seawater than in distilled H_2O, which caused the lower reaction rate.

4.6. Crack and surface area effects on LiH–H_2O reaction kinetics

In the experimental literature reviewed, many authors did not specify whether their samples were crack-free, contained microcracks, or contained some other type of porous microstructure. The presence of cracks or porosity could have a large effect on reaction kinetics, because they would provide pathways through product layers for oxygen containing species to react with subsurface LiH. Polycrystalline LiH would clearly have grain boundaries, which could potentially act as diffusion pathways. Surface area effects on reaction rates should be somewhat analogous to crack effects, because the presence of cracks provides more surface area for reaction. Therefore, surface area studies are also discussed in this section.

Two studies showed that microcracks did not form in LiOH (at either unspecified or low H_2O concentrations). Myers studied the effects of LiOH on rates of reaction between LiH and Te [49]. Myers found that LiOH formed on single crystal LiH served as a barrier to reactions until the LiOH was compromised by volume contractions during

conversion to Li_2O at elevated temperatures. Unfortunately, the conditions for formation of the LiOH were not stated and no description was given of the microstructure. Holcombe [40] completed an SEM study of hydrolyzed polycrystalline LiH exposed to 317 Pa of H_2O in Ar at RT (we assume) for 42 000 min. No microcracks were observed for images up to 30 000 times magnification. The authors concluded that the LiOH crystalline structure was sufficiently open to allow easy diffusion of an oxygen-containing species. They furthermore reasoned that the rate-controlling step for LiH hydrolysis takes place at the LiOH/LiH interface.

Results were also obtained, including some by Holcombe and Powell [10], that showed the presence of microcracks on hydrolyzed LiH. Holcombe and Powell completed SEM studies of hydrolyzed {1 0 0} LiH single crystal exposed to ~1268 Pa of H_2O in air at RT for ~259 200 min (~6 months) [10]. A description of the microstructure stated that preferential hydrolysis had taken place at the sample corners and that the LiOH layer contained cracks. Subsequent heating of the sample at 75 °C caused cracks to appear in the LiH also, however, there were no cracks at the LiOH/LiH interface. Balooch et al. [16] identified cracks in product layers on {1 0 0} single crystal LiD exposed to air containing 1584 Pa H_2O at RT for ~3400 min by using SEM. The cracks formed at the corner of a sample with a hydrolysis layer several microns thick. Dinh et al. [27] showed an SEM microstructure of single crystal LiD hydrolyzed at ~600–1000 Pa H_2O in air that contained columnar structures with voids and open spaces between the columns. Both Balooch et al. and Dinh et al. suggested that the cracks or open spaces could provide pathways for migration of an oxidizing species to a reaction interface.

The H_2O exposure concentration is an interesting difference between the 1972 experiment by Holcombe [40] and the other experiments just discussed [10,16,40]. The Holcombe experiment [40], in which no microcracking was observed, was the only experiment that clearly used H_2O concentrations at a level that should form LiOH (317 Pa). The H_2O concentrations of the other experiments were sufficient to form $LiOH \cdot H_2O$. The higher H_2O concentrations may have resulted in stresses and cracking not present at lower H_2O concentrations. Also, if conditions were sufficient to revert the $LiOH \cdot H_2O$ to LiOH, then a porous microstructure may have resulted. A porous microstructure would not necessarily be present in a LiOH microstructure that was not converted from $LiOH \cdot H_2O$, such as the polycrystalline sample treated at 317 Pa H_2O by Holcombe.

Holcombe and Powell also calculated the strain that occurs between LiOH and LiH as a result of lattice mismatch [10]. The average percentage of strain was calculated to be 6.8%, assuming that the strain was equally shared between LiH and LiOH. They conjectured that a transition region between the two structure types was present at the LiOH/LiH interface, which reduced the strain between them. The authors stated that the transition region is 'perhaps no wider than the 300 Å SEM resolution limit' and apparently reduces strain at the formation temperature of the layers, but would not be sufficient to eliminate microcrack-producing strains at other temperatures. Although the authors did not speculate on the composition of this 'transition region,' it could be a Li_2O layer. When the strain calculation is completed for an Li_2O/LiH interface, the value is 6.5%, slightly less than the strain value of 6.8% calculated for LiOH/LiH.

Two studies noted that $LiOH \cdot H_2O$ is relatively impervious to reaction with H_2O because of its compacted microstructure. The first researcher was de Pablo [50], who used thermogravimetric analysis to determine that $LiOH \cdot H_2O$ does not fully rehydrate after being heated (to remove H_2O) and then cooled. He presented XRD data, which indicated that hydrolyzed material contained both $LiH \cdot H_2O$ and LiOH. Further, he presented SEM micrographs showing hydrolyzed material with no porosity, which he deemed 'impenetrable.' de Pablo reasoned that the increase in molar volume of $LiOH \cdot H_2O$ over that of LiOH (27.8 cm^3/mol for $LiOH \cdot H_2O$ and 16.5 cm^3/mol for LiOH) was sufficient to cause this effect. A study by Kong et al. [43], showed that LiH particles would not hydrolyze to produce their full capacity of H_2. Kong et al. suggested that the hydrolyzed microstructure (i.e. $LiOH \cdot H_2O$) would not allow passage of an oxidizing species to the interior of the LiH bed for further reaction. They presented SEM micrographs of the hydrolyzed LiH particles showing an agglomerated microstructure with no pores or gaps. While both de Pablo and Kong et al. concluded that the hydrolyzed microstructure was sufficiently compacted to disallow further reaction with H_2O on the time scale of their experiments (up to several thousand min), the $LiOH \cdot H_2O$ crystal structure has relatively large open spaces and may allow diffusion of an oxidizing species intragranularly on a much slower time scale.

Also, heavily hydrolyzed LiH has been observed to spall, which may provide fresh surface area for hydrolysis.

In gravimetric studies of LiH exposed to moist Ar, Broughton reacted fine particle LiH (up to a 2 mm maximum particle diameter with a wide size distribution), coarse particle LiH (up to 5 mm maximum particle diameter), and a pellet containing pressed fine particle LiH. The three types of materials were each tested in two environments: Ar carrying 1.3 kPa H_2O flowing at 1000 mL/min at 33 °C, and Ar carrying 0.95 kPa of H_2O flowing at 1000 mL/min at 39 °C (all at glovebox pressures). Results are given in Fig. 24. The experiments both showed that the fine particle material (high surface area) resulted in the greatest rate of reaction followed by the coarse particle and then pellet, each having consecutively lower surface areas.

DeVries et al. [41], Pitcher et al. [42], and Kong et al. [44] all studied the effects of LiH surface area on hydrolysis rates. DeVries intimately mixed polycrystalline LiH particles of varying sizes with liquid H_2O, while Pitcher et al. exposed LiH polycrystalline pellets of varying sizes to flowing distilled H_2O vapor, and Kong et al. exposed polycrystalline LiH pieces of varying sizes (particles, granules, and lumps) to distilled H_2O vapor. All researchers found that increasing the surface area increased reaction rates. Kong et al. further showed that for hydrolysis of CaH_2, the linear slope of the H_2 production vs. time curve was dependent on surface area available for reaction. This effect is illustrated in Fig. 28. Similar results could be expected for LiH.

The importance of sample surface area can further be seen by inclusion in reaction rate models for LiH hydrolysis. Kong et al. [44] included sample dimensions in their model. Leckey et al.'s [45] model included time dependent sample surface area. Leckey et al. also calculated the effect of sample rounded edges (rather than sharp edges) on reaction rates, but found that the rounded corner effect was not significant.

4.7. Kinetics for reactions between LiH hydrolysis products

Newton et al. [6] determined gas evolution rates for the $LiH + LiOH \rightarrow Li_2O + H_2$ reaction by heating pellets of a 50/50 mol% mix of LiH and LiOH at two temperatures and collecting the evolved gas (attributed to H_2) for 2700 min. The pressure remained constant during the last 1440 min of heating. At 240 °C, the gas evolution rate was 3.25×10^{-2} mmol/h. At 150 °C, a rate of 1×10^{-3} mmol/h was estimated, although this rate was considered too low to be accurately measured. Gas was also evolved at RT. Heating pellets to temperatures 100–295 °C significantly reduced the subsequent amount of gas evolution at RT, indicating that the reaction to form Li_2O and evolve H_2 had already been driven nearly to completion as a result of the heating.

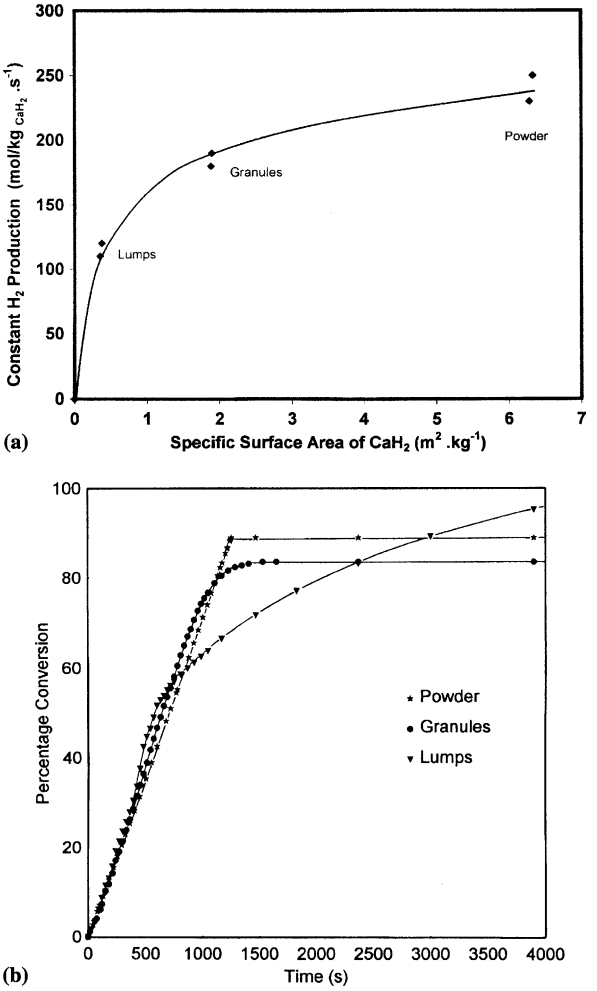

Fig. 28. Effect of surface area for CaH_2 hydrolysis as demonstrated by (a) H_2 production as a function of time and (b) H_2 production rate as a function of surface area [44].

Frazer [31] measured the H_2 concentration released from samples of LiH polycrystalline pellets with small additions (typically a few weight percent) of LiOH during heating in vacuum. The measured H_2 was used to quantify the LiOH, per the reaction $LiH + LiOH \rightarrow Li_2O + H_2$. The H_2 volume was measured; the gas was not chemically identified.

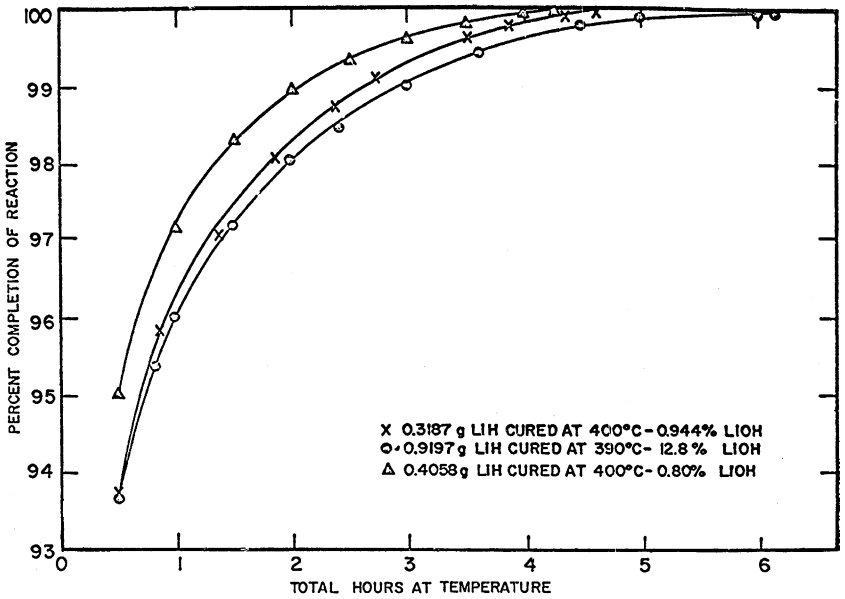

Fig. 29. H_2 production from pellets of LiH/LiOH mixtures heated at 390 °C and 400 °C in vacuum [31].

Fig. 29 shows the curves for reactions at 390 °C and 400 °C. The reaction proceeds very quickly for the first few hours and then rapidly slows; no equation was developed for the reaction rate.

Broughton [15] completed measurements that were similar to Frazer, in which polycrystalline pellets of LiH held in vacuum at temperature (30 °C, 60 °C, or 120 °C) and evolved H_2 gas measured. In Broughton's study, however, the gas product was attributed to H_2 by the direct hydrolysis reaction $LiH + H_2O \rightarrow LiOH + H_2$. It is not clear why this reaction was considered to take place rather than the reaction identified by Frazer, $LiH + LiOH \rightarrow Li_2O + H_2$, in which small amounts of contaminant LiOH would react with the LiH sample; Broughton may have expected the former reaction at the low temperature range ($\leqslant 120$ °C) of the experiment. It is also unclear what was the source of H_2O for the long time periods of the experiments (months to years). Activation energies were determined to be 230–250 kJ/mol and 80–100 kJ/mol for energies determined from peak and equilibrium outgassing rates respectively. Broughton determined that measurable outgassing decreased over the time periods studied and that the rates were greater at increased temperatures. Fig. 30 shows instantaneous outgassing rates of H_2 as a function of time at 120 °C for several LiH prepared by several methods. The rates decreased for material that was initially treated at higher temperatures. Also, the Li-rich sample showed notably less outgassing of H_2. This would indicate that excess Li bonds with available hydrogen. Data for LiH held at 30 °C and 60 °C showed the same trends as for 120 °C. A typical rate was determined to be (1×10^{-6} mol H_2/mol LiH)/day, although Broughton believed that the method of instantaneous outgassing did not give good quantitative values.

In Myers RBS study in which a LiOH/LiH single crystal was heated to 280 °C in vacuum [11], he concluded that the Li_2O was produced at two reaction fronts: one front at the sample surface ($2LiOH \rightarrow Li_2O + H_2O$) and the other front at the LiOH/LiH interface ($LiH + LiOH \rightarrow Li_2O + H_2$). Fig. 31 shows the rate of conversion of O atoms to a form tied up in Li_2O at 200 °C and 250 °C. The rates were estimated to be linear. Examination of the data shows that the reaction at 250 °C took ~4 h to complete, while the reaction at 200 °C took >100 h (much longer) to complete. The reaction rates were determined to be $\sim 5 \times 10^{14}$–5×10^{16} atoms/cm^2 s over the temperature range of 200–280 °C, which is a difference of approximately two orders of magnitude. Myers determined a temperature dependence for the LiOH to Li_2O conversion, which is shown in Fig. 32, by using his data along with data of other researchers. He notes that for a closed system there is a large variation in the equilibrium H_2O concentration present over LiOH/Li_2O for the experiment temperatures which likely causes the

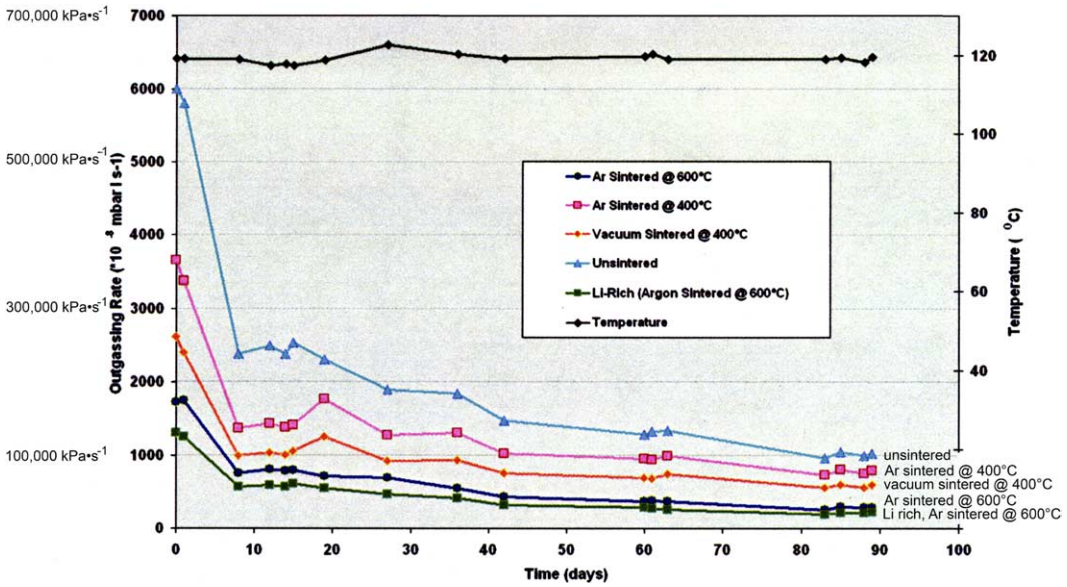

Fig. 30. Outgassing rate from pellets of LiH heated at 120 °C in vacuum [15]. SI units and curve labels were added by the present authors.

large temperature dependence of the reaction rate; the H_2O concentrations are 2.1×100^{-1} Pa at 280 °C and 1.7×10^{-3} Pa at 200 °C. Myers gave an expression for the growth of Li_2O in Eq. (12), which he considered to be equal to the rate of adsorption of H_2O.

$$S = \gamma P_{H_2O}(2\pi k_B m T)^{-\frac{1}{2}}, \tag{12}$$

S = rate of adsorption of H_2O molecules; γ = fraction of H_2O retained molecules; $P_{H_2O} = H_2O$ pressure; k_B = Boltzmann constant; m = mass of H_2O molecule; T = temperature. The activation energy calculated for the conversion was 130 kJ/mol. Myers concluded that reactions at the two fronts were the rate limiting steps in the process. Holcombe and Powell [10] agreed with the previous statement; they concluded that the LiOH to Li_2O conversion was not controlled by diffusion of H_2O, but by reaction at the LiOH/LiH interface [10].

Kudo [51] determined reaction rates for $2LiOH \rightarrow Li_2O + H_2O$ and analogous LiOD and LiOT reactions by heating the samples and using mass spectroscopy, weight changes, and radiation detection (for T reactions) for analysis. The samples were polycrystalline particles; the temperature range of the measurements was 257–417 °C. The reaction rates were determined to be first order in the quantity of released water. Calculated rate constants in units of s^{-1} were $k_{H_2O} = 1.8 \times 10^8 \exp(123\,500/RT)$,

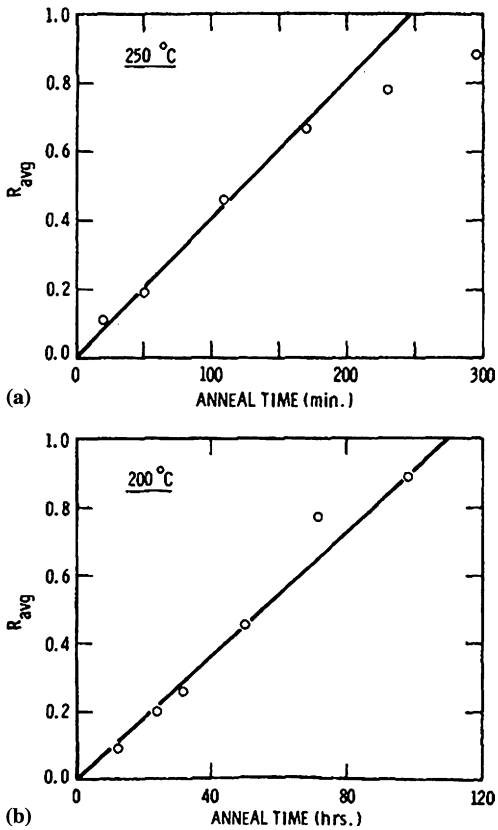

Fig. 31. Time dependence for the conversion of LiOH to Li_2O at (a) 250 °C and (b) 200 °C. R = local fraction of O tied up in Li_2O [11].

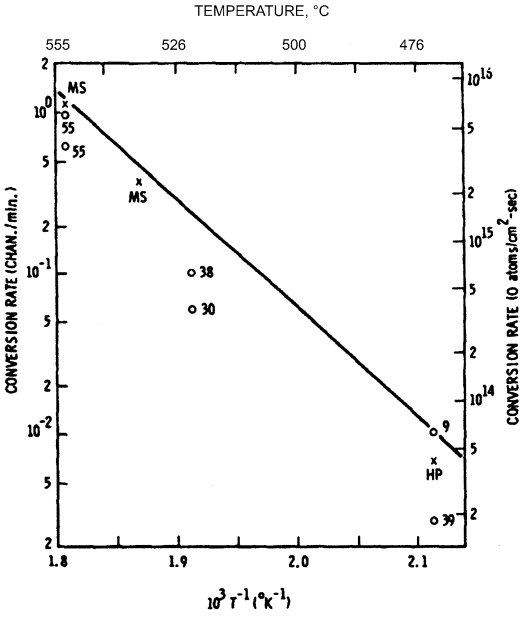

Fig. 32. Temperature dependence of the conversion rate of LiOH to Li_2O. Circles are data from Myers [11]; crosses are rate deduced from McIntyre and Smith [21] (MS), and Holcombe and Powell [10] (HP). The solid line was calculated from the equilibrium dissociation pressure of H_2O over LiOH/Li_2O [11].

$k_{D_2O} = 1.7 \times 10^8 \exp(121\,400/RT)$, and $k_{HTO} = 1.6 \times 10^7 \exp(128\,500/RT)$, where R is the gas constant (J/mol K) and T is temperature (K). The reaction involving T was assumed to be LiOH + LiOT → Li_2O + HTO, i.e. the water product contained both protium and tritium, because analysis showed that the reactant hydroxide contained a high concentration of protium. The rate constants for H_2O and D_2O are very similar, but the rate constant for HTO is approximately one order of magnitude smaller. The behavior for mixed isotope water may be more complex than behavior for single isotope waters. Using the Arrhenius equation (Eq. (9)), the calculated activation energy for the decomposition reactions was 124 kJ/mol, with no significant differences observed for the effect of different hydrogen isotopes; pre-exponential factors were 0.918, 0.915, and 0.858 1/s for decomposition of 2LiOH, 2LiOD, and LiOH + LiOT respectively.

McIntyre and Smith [21] completed a thermogravimetric kinetic study of LiOH particles in which LiOH was heated isothermally between 200 and 400 °C in vacuum. The data were fit to a shrinking core model given in Eq. (13), as follows:

$$(1-\alpha)^{\frac{1}{3}} = 1 - \frac{kt}{R}, \tag{13}$$

α = reacted fraction; k = rate constant; R = particle radius; t = time.

McIntyre and Smith concluded that the reaction proceeds at a linear rate by the advance of a two-dimensional reaction interface, provided that the H_2O vapor pressure maintained over the material is a least several orders of magnitude lower than the equilibrium pressure of H_2O over the LiOH–Li_2O system. An activation energy for the reaction 2LiOH → Li_2O + H_2O was calculated to be 93 kJ/mol. SEM micrographs of the LiOH particles showed that they contained cracks.

Using TPD, Dinh et al. [20] determined appropriate rate expressions and quantified parameters for reactions occurring during heating of LiOH · H_2O. The first reaction to occur with heating is removal of the H_2O, which Dinh et al. described by Eq. (13) given below. E was determined to be 47–68 kJ/mol and v was ~10^6 1/s.

$$\alpha(t) = 1 - \exp\left[-tve^{-(E/RT)}\right], \tag{14}$$

α = reacted fraction; t = time; R = gas constant, T = temperature; v = pre-exponential factor; E = activation energy.

At higher temperatures, LiOH decomposes by the reaction 2LiOH → Li_2O + H_2O. Eq. (13), as well as two further rate expressions (Eqs. (15) and (16)), were found applicable for this reaction and are given below.

$$\alpha(t) = 1 - \left\{1 - \left[\frac{v}{3}te^{-(E/RT)}\right]\right\}^3, \tag{15}$$

α = reacted fraction; t = time; v = pre-exponential factor; E = activation energy; R = gas constant, T = temperature.

$$\alpha(t) = 1 - \left\{\left[1 - \frac{\kappa}{r}\left(\frac{T-T_0}{\beta}\right)\right]^2\left[1 - \frac{\kappa}{Z}\left(\frac{T-T_0}{\beta}\right)\right]\right\}, \tag{16}$$

α = reacted fraction, t = time, T = temperature; r = average radius of hydrolysis structure; Z = average height of hydrolysis structure; β = heating rate; $\kappa = \kappa_0 e^{-(E/RT)}$; E = activation energy, R = gas constant.

The measured activation energies varied from 86 to 142 kJ/mol, with pre-exponential factors of ~10^6–10^9 1/s. The wide variation in activation energies was attributed to lower activation energies for defective LiOH, such as might be found at an interface. The range of activation energies led to projected LiOH stability time frames ranging from

decades to over a century at *RT*. The reaction $LiOH + LiD \rightarrow Li_2O + H_2/HD/D_2$ was also determined to also occur during heating of LiOH/LiD. The authors concluded that LiOH molecules must diffuse through Li_2O for this reaction to occur and developed an expression for the diffusion coefficient of LiOH (Eq. (17)). In a dry environment at *RT*, the diffusion coefficient was determined to be $\sim 1 \times 10^{-23}$ m^2/s.

$$D = 4.1467 \times 10^{-16} \exp\left(\frac{-44\,929}{8.314T}\right), \tag{17}$$

D = diffusion coefficient, m^2/s; T = temperature.

From DTA and TGA experiments performed by Popescu et al. [38] on $LiOH \cdot H_2O$, reaction parameters for both the hydrate and hydroxide decomposition reactions were measured for use in Eq. (18):

$$\ln(1-\alpha) = -\frac{E}{RT} + \ln\frac{A}{b} + L, \tag{18}$$

α = reacted fraction; E = activation energy, kJ/mol; R = gas constant, kJ/mol; T = temperature, K; A = pre-exponential factor, 1/s; b = heating rate, K/s; L = correction factor.

Reaction parameters for the reaction $LiOH \cdot H_2O \rightarrow LiOH + H_2O$ were determined to be: reaction order = 1, $E = 63$ kJ/mol, and $A = 10^7$ 1/s. Reaction parameters for the reaction $2LiOH \rightarrow Li_2O + H_2$ were determined to be: reaction order = 1, $E = 101$ kJ/mol, and $A = 10^3$ 1/s. The activation energy value of 101 kJ/mol is the range of values obtained by other researchers for the LiOH decomposition reaction [11,20,21,34,38,51].

Using TPD and diffuse reflectance IR, Kopasz et al. [34] were able to determine qualitative kinetic information for Li_2O heated to elevated temperatures. An IR spectra for sample as it was heated at 400 °C in Ar + 0.1 mol% H_2 (forming LiOH) showed decay of a 3657 cm^{-1} peak (the main peak for LiOH), indicating first order desorption of LiOH ($2LiOH \rightarrow Li_2O + H_2O$). The authors claimed that the decay was an order of magnitude slower than reported for reaction of bulk LiOH; however, no values were given, and no reference was given regarding bulk LiOH data. Dinh et al. also found that 'defective' LiOH (prepared by hydrolyzing LiD) acted differently than bulk LiOH; defective LiOH decomposed at lower temperatures than bulk LiOH [27]. Kopasz et al. analyzed a further sample of Li_2O by heating in Ar + 0.1 mol% H_2 (forming LiOH). The TPD spectrum showed the presence of a peak (presumably H_2O) simultaneous to the decay of a LiOH IR peak at 3657 cm^{-1}. Further, as the 3657 cm^{-1} peak substantially decayed, an Li–H peak was formed. The authors concluded from combined TPD and IR data, that the 3657 cm^{-1} was OH species being removed from the sample surface. The location on the surface, along with the observed change in species concentration with time, led the authors to additionally conclude that bulk diffusion was not the rate-controlling mechanism for disappearance of the 3657 cm^{-1} LiOH peak.

In further experiments by Kopasz et al. [34], Li_2O was heated at 250 °C while being purged with D_2 for 180–1440 min (creating some LiOD). The purge gas was then changed to an Ar + 0.1 mol% H_2 mixture, and the sample was heated up to 1000 °C while measurements were taken. The TPD spectrum showed one main peak at 600–700 °C, as well as a peak at ~800–1000 °C. The main peak was identified as desorption of OD, i.e. $2LiOD \rightarrow Li_2O + D_2O$, with a calculated activation energy of 102.5 kJ/mol (determined by a plot of $\ln(T_m^2/H)$ vs. $1/T_m$ where T_m is peak maximum temperature and H is the heating rate). The authors stated, however, that line-shape analysis of the peak indicated a higher activation energy than determined by the peak maximum temperature and that the reaction was not first-order desorption, as seen in their previous experiment at 400 °C.

Fig. 33 shows data resulting from the experiments of Nishikawa et al. [32] in which Li_2O particles were heated to 500–700 °C while 400 mL/min He/H_2 gas was passed through a Li_2O bed. Reactant H_2 and product H_2O concentrations were measured. The figure shows the instantaneous H_2 and

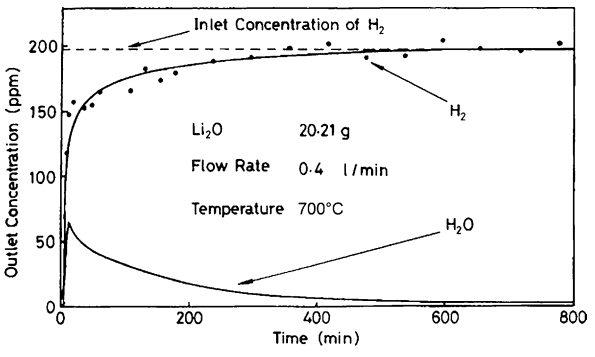

Fig. 33. Change of H_2 and H_2O concentration with time for the outlet gas of Li_2O treated with flowing $He + H_2$ at 700 °C [32]. The units for gas concentration were not identified in the reference.

H_2O concentrations (at the experiment outlet) with time. The H_2 concentration is initially low at the outlet, as a large quantity is being used in the reaction; the curve for the H_2O concentration has a symmetrically opposite shape in which the concentration decreases with time because the reaction has slowed [52]. A equation for the temperature dependence for the formation of H_2O (and consumption of H_2) was determined, as shown in Eq. (19) to be $\Delta H_2O = 3.12 \times 10^{-3} \exp(-49\,404/RT)$, where ΔH_2O is the amount of H_2O generated per gram of Li_2O, and T is temperature in K. The identity of the reaction that forms H_2O was not clear.

$$\Delta H_2O = 3.12 \times 10^{-3} \exp\left(\frac{-49\,404}{RT}\right), \tag{19}$$

ΔH_2O = amount of H_2O; generated per g of Li_2O; R = gas constant, J/(mol K); T = temperature, K.

A number of studies have focused on the conversion of LiOH to Li_2O. Specifically, the $2LiOH \rightarrow Li_2O + H_2O$ reaction has been described as first order, shrinking core, and with more complex equations. Calculated activation energies included ranges of 93–130 kJ/mol as determined by several researchers [11,21,34,38,51] and 83–149 kJ/mol [20,27] as determined by Dinh et al. These values were specified for the specific reaction $2LiOH \rightarrow Li_2O + H_2O$ (or an isotopic variant), except in one case where Myers specified two simultaneous reactions, the previous as well as $LiH + LiOH \rightarrow Li_2O + H_2$ (sum of two reactions) [11]. Dinh et al. theorized that the large range of activation energies is a result of the decomposition of better and worse (a more defective structure) LiOH. More defective LiOH has a lower activation barrier to decomposition, while less defective LiOH has a greater activation barrier. Microstructural or other direct evidence of defect concentrations would help support this concept. Some studies of the reaction to form Li_2O were completed with lithium hydride present, while others presumably did not have the compound present. Except for the Myers study, the identification of the $2LiOH \rightarrow Li_2O + H_2O$ reaction resulted from the identification of H_2O, in cases where both LiOH and hydride were present.

5. Conclusions

A large number of studies on LiH hydrolysis exist. These studies were completed by a variety of research groups under a wide range of experimental conditions. Comparison of the results is difficult, particularly as LiH hydrolysis is not limited to just one reaction, but several. Indeed, researchers are not in agreement as to which reactions take place. It is clear that LiH hydrolysis products may include Li_2O, LiOH, $LiOH \cdot H_2O$, and potentially other Li–O–H compounds (as well as compounds formed from impurities), that have some mutual solubility and depend, at least to some degree, on the level of H_2O exposure.

Three researcher groups (Machin and Tompkins [12], Phillips et al. [13] and Tanski [14]) concluded that Li_2O forms prior to LiOH. Machin and Tompkins concluded that when LiH is exposed to very-low H_2O concentrations (specified as <1 monolayer of H_2O), only Li_2O is formed. With larger doses of H_2O, Li_2O is formed as an intermediary to the final and only product, LiOH. It is unnecessary, however, to assume that LiOH is the only product from large H_2O doses; a Li_2O layer, if very thin as projected, could be present in the hydrolysis product structure. Li_2O, in fact, has been shown to be present simultaneously with LiOH.

Reasonably good agreement exists regarding the relative locations of hydrolysis product layers. The 'shorter'-term (to years) end result of the LiH hydrolysis process at RT and ambient pressure is $LiOH \cdot H_2O/LiOH/Li_2O/LiH$ (bulk). Thus, the dilemma of whether the 'oxide first' scenario or whether the 'hydroxide first' scenario occurs, may not matter for many applications.

The kinetic expressions for formation of hydrolysis products depend on how many hydrolysis products are formed. Thus, reaction rates should be compared with care. Despite this, studies of LiH hydrolysis kinetics with a continuous supply of H_2O in the 'high H_2O regime' overwhelmingly showed a linear rate of reaction for formation of LiOH and $LiOH \cdot H_2O$. The slope, and to some degree shape, of each product concentration vs. time curve depends strongly on the conditions of the experiment, e.g. pressure, temperature, and sample surface area. Kong et al. [44], in particular, showed that sample surface area is a significant parameter.

In many instances (but not all), the hydrolysis reaction rate has also been described as diffusion controlled [10,15,16,40,44,46]. A diffusion controlled process, in which the diffusion occurs through a thin layer, will result in a linear reaction rate. Moreover, a thin layer diffusion concept fits nicely with a hydrolysis product structure consisting of layers. Some authors have attributed LiH–H_2O

linear reaction rates to microcracking or rapid lattice diffusion [10,12]; while these mechanisms may play a role, it should also be recognized that overall linear kinetics may result from a diffusion controlled reaction in which the rate controlling step is diffusion across a thin layer. Some researchers considered the oxidant diffusant to be H_2O, however, the mobile species was not usually identified.

A variety of results were obtained for the dependence of LiH–H_2O reaction rates on temperature and pressure. The dependencies can potentially be explained in terms of diffusion across hydrolysis layers, in which the layers vary in proportion (i.e. thickness) with temperature and pressure. The result is varying times for diffusion across the layers. Specific explanations for a temperature or pressure effect would depend on the specific experimental variables and resulting phase concentrations. However, it is clear that if the thickness of a layer that controls kinetics were to increase dramatically with increasing temperature (while other variables were kept constant) a decreasing reaction rate would be observed.

LiH hydrolysis products appear to readily react amongst themselves under the appropriate conditions. The most studied reactions of this genre are the reactions that form Li_2O. Over the long term (many years) and in dry environments, it appears that Li_2O is formed from LiOH, along with LiH if available ($2LiOH \rightarrow Li_2O + H_2O$ and $LiOH + LiH \rightarrow Li_2O + H_2$). Most studies used elevated temperatures to study these reactions, as they occur more quickly at greater temperatures. However, one study does give evidence that Li_2O may form at RT [6], and another study projected that Li_2O formation may continue for decades at RT [27]. This may lead to concerns for the long-term stability of impure polycrystalline LiH and the desire to eliminate LiOH if the Li_2O-producing reactions cannot be tolerated. Activation energies for oxide forming reactions were determined and several kinetic expressions applied.

Numerous LiH hydrolysis reactions can occur, as well as reactions among the hydrolysis products. Products in the Li–O–H system have been demonstrated to readily change, dependent upon the environmental conditions. In light of the highly reactive nature of LiH and the Li–O–H compounds, thermodynamic data for the reactions should be thoroughly compiled and the temperature-pressure-concentration regions of phase stability should be determined. This information, in conjunction with kinetic data, would be useful to predicting the reactions and products that occur as LiH reacts with H_2O.

Acknowledgements

The authors would like to acknowledge Duncan Broughton, Long Dinh, Jonathan Phillips, and John Tanski for insight and discussions of LiH reactions. We also appreciate the efforts of the many authors of the literature reviewed; we have attempted to convey the information from these works correctly, but we apologize for any errors that may have been made.

References

[1] M. Guntz, Comp. Rend. 123 (1896) 694.
[2] T. Mel'nikova, High Temp.–High Press. 13 (1981) 675.
[3] S. Stecura, J. Less Common Met. 33 (1973) 219.
[4] Powder Diffraction File 4/Full File 2004, 00-032-0564, 00-025-0486, 03-065-3972, International Centre for Diffraction Data, 2004.
[5] CRC Handbook of Chemistry and Physics, 66th Ed., Chemical Rubber Company, Boca Raton, FL, 1985–1986, p. F-156.
[6] T. Newton, G. Challenger, C. Holley, M. Alei, E. Head, A. Zalkin, T. Ready, A. Florin, T. White, S. Shlaer, Miscellaneous Information on the Properties and Handling of LiH and Li(D,T), Los Alamos Scientific Laboratory report, LAMS-1074, Los Alamos Scientific Laboratory, 1954.
[7] N. Smyrl, E. Fuller, G. Powell, Appl. Spectrosc. 37 (1983) 38.
[8] J. McLaughlin, S. Cristy, Composition of corrosion films on lithium hydride surfaces after exposure to air, Oak Ridge Y-12 Plant report Y-1929, Oak Ridge Y-12 Plant, 1974.
[9] S. Cristy, SIMS depth profiling of an insulating air-sensitive material, Oak Ridge Y-12 Plant report Y/DW-725, Oak Ridge Y-12 Plant, 1987.
[10] C. Holcombe, G. Powell, J. Nucl. Mater. 47 (1973) 121.
[11] S. Myers, J. Appl. Phys. 45 (1974) 4320.
[12] W. Machin, F. Tompkins, Trans. Faraday Soc. 62 (1966) 2205.
[13] J. Phillips, M. Bradford, M. Klanchar, Energy & Fuels 9 (1995) 569.
[14] J. Tanski, Analysis of a New Reaction Mechanism for Hydrolysis of LiH, Los Alamos National Laboratory, LAUR-00-5324, 2000.
[15] D. Broughton, Hydrolysis of lithium hydride, PhD thesis, The University of Reading, Reading, UK, 2001.
[16] M. Balooch, L. Dinh, D. Calef, J. Nucl. Mater. 303 (2002) 200.
[17] Messer, J. Am. Chem. Soc. 77 (1955) 4524.
[18] JANAF Thermochemical Tables, Dow Chemical Company, 1971.
[19] J. Berkowitz, D.J. Meschi, W.A. Chupka, J. Chem. Phys. 33 (1959) 533.
[20] L. Dinh, W. McLean, M. Schildbach, J. LeMay, W. Siekhaus, M. Balooch, J. Nucl. Mater. 317 (2003) 175.

[21] J. McIntyre, H. Smith, American Chemical Society abstract for the S.E. and S.W. Regional Meeting, 1970, p. 174.
[22] M. Tetenbaum, A. Fisher, C. Johnson, Fusion Technol. 7 (1985) 53.
[23] J. Norman, G. Hightower, J. Nucl. Mater. 122&123 (1984) 913.
[24] O. Krikorian, High Temp.–High Press. 20 (1988) 183.
[25] T. Terai, H. Mohri, Y. Takahashi, J. Nucl. Mater. 179–181 (1981) 808.
[26] Y. Ueda, The Science Reports of the Tohoku Imperial University–First Series, vol. 22, 1933.
[27] L. Dinh, M. Balooch, C. Cecala, J. Leckey, J. Nucl. Mater. 295 (2001) 193.
[28] G. Powell, M. Milosevic, J. Lucania, N. Harrick, Appl. Spectrosc. 46 (1992) 111.
[29] H. Johnston, T. Bauer, J. Am. Chem. Soc. 73 (1951) 1117.
[30] CIS-International Occupational Health and Safety Information Centre, Material Safety Data Sheet for LiOH, 2004.
[31] J. Frazer, Analysis and Destruction of Lithium Hydroxide in Lithium Hydride, University of California Radiation Laboratory–Livermore Site report UCRL-5133, 1958.
[32] M. Nishikawa, Y. Kawamura, K. Munakata, K. Yoneda, J. Nucl. Mater. 174 (1990) 121.
[33] E. Shpil'rain, Thermophysical Properties of Lithium Hydride, Deuteride, and Tritide and of Their Solutions with Lithium, American Institute of Physics, New York, 1987, p. xii.
[34] J. Kopasz, J. Ortiz-Villafuente, C. Johnson, An Investigation of the Desorption of Hydrogen from Lithium Oxide using Temperature Programmed Desorption and Diffuse Reflectance Infrared Spectroscopy, Argonne National Laboratory report ANL/CMT/CP 83894, Argonne National Laboratory (1994).
[35] H. Beutler, G. Brauer, Die Naturwissensch. 24 (1936) 347.
[36] R. Buchanan, W. Bowen, J. Chem. Phys. (1960) 349.
[37] Y. Furuyama, K. Ito, S. Dohi, A. Taniike, A. Kitamura, J. Nucl. Mater. 313–316 (2003) 288.
[38] C. Popescu, R. Jianu, R. Alexandrescu, I. Mihailescu, I. Morjan, J. Pascu, Thermochim. Acta 129 (1988) 269.
[39] T. Gibb Jr., C. Messer, A Survey Report on Lithium Hydride, Atomic Energy Commission report NYO-3957, Tufts College, 1954.
[40] C. Holcombe, Retardation of the Reaction of Lithium Hydride with Water Vapor, Oak Ridge Y-12 Plant report Y-1835, Oak Ridge Y-12 Plant, 1972.
[41] G. DeVries, Pyrodynamics 6 (1968) 147.
[42] G. Pitcher, G. Kavarnos, Int. J. Hydrogen Energy 22 (1997) 575.
[43] V. Kong, R. Foulkes, D. Kirk, J. Hinatsu, Int. J. Hydrogen Energy 24 (1999) 665.
[44] V. Kong, R. Foulkes, D. Dirk, J. Hinatsu, Int. J. Hydrogen Energy 228 (2003) 205.
[45] J. Leckey, L. Nulf, J. Kirpatrick, Langmuir 12 (1996) 6361.
[46] V. Rozenband, Int. Chem. Eng. 15 (1975) 456.
[47] C. Cecala, S. Shaw, J. Leckey, Y-12 National Security Complex report Y/DZ-2304, BWXT/Y-12 National Security Complex, 2001.
[48] ASTM D 1141-98, Standard Practice for the Preparation of Substitute Ocean Water, 2003.
[49] S. Myers, J. Appl. Phys. 48 (1977) 4777.
[50] J. de Pablo, Thermochim. Acta 113 (1987) 87.
[51] H. Kudo, J. Nucl. Mater. 87 (1979) 185.
[52] M. Nishikawa, Y. Kawamura, K. Munakata, K. Yoneda, J. Nucl. Mater. 187 (1992) 153.
[53] W. Oates, Imperial College Report for AWE for the Period January–June 1964 and June–December 1964.
[54] N. Segal, Imperial College Final Report for AWE: October 1965–September 1966.
[55] R. Mather, Imperial College Report for AWE to September 1971.